Insulin Receptor Substrate 2 is Required for Testicular Development

Richard J. Griffeth

A thesis presented for the Degree of Doctor of Philosophy (Ph.D.)

Molecular Neuroendocrinology Laboratory
Centro de Investigación Príncipe Felipe
Valencia, Spain

and

Department of Animal and Food Science
Autonomous University of Barcelona
Bellaterra, Spain

September 2012

September 2012

We hereby recommend that the doctoral thesis prepared under our supervision at the Centro de Investigación Príncipe Felipe (Valencia, Spain) by Richard J. Griffeth entitled "Insulin Receptor Substrate 2 is Required for Testicular Development" be accepted as fulfilling the requirements for the Degree of Doctor of Philosophy (Ph.D.) at the Universidad Autónoma de Barcelona (Bellaterra, Spain).

_____

Richard J. Griffeth

_____

Deborah J. Burks, Ph.D.
Thesis Supervisor - Centro de Investigación Príncipe Felipe (Valencia, Spain)

_____

Maria Teresa Paramio Nieto, Ph.D.
Thesis Tutor - Universidad Autónoma de Barcelona (Bellaterra, Spain)

Table of Contents

Abstract (English)

Insulin receptor substrate (IRS) proteins are key mediators of insulin and insulin-like growth factor (IGF) 1 signaling. In mice, deletion of *Irs2* causes diabetes and females are infertile. However, the role of IRS2 in male reproduction is unknown. Therefore, the objectives of these studies were to determine if *Irs2*-deficiency alters testicular development and function. *Irs2*-deficient adult and neonatal male mice exhibited reduced testicular size and weight. There was a reduction in the number of Sertoli cells, spermatogonia, spermatocytes, and spermatozoa, however there were no differences in the number of Leydig cells or the concentration of testosterone in serum. Testicular morphology appeared unaffected, and there were normal cellular associations without obvious abnormalities in the seminiferous epithelium. Gene and protein expression of IRS1, 3, and 4 were unchanged in *Irs2*-deficient mice indicating that the other IRS proteins did not overcompensate for the loss of *Irs2*. Gene expression of growth hormone receptor and protein expression of SOX9 were significantly reduced in *Irs2*-deficient mice. There was increased phosphorylation of AKT, GSK3β, and ERK in the testes of *Irs2*$^{-/-}$ mice but no differences in protein expression of cell cycle regulatory proteins cyclin D or p27. In summary, the results from these studies demonstrate that IRS2 plays a critical role in the regulation of testis size, and that IRS2 may modulate testis size by reducing or delaying Sertoli cell proliferation during embryonic and early postnatal development. These results provide an important platform for further understanding the effects of IRS2 signaling and diabetes on male reproductive function.

Resumen (Español)

Las proteínas sustrato del receptor de insulina (de sus siglas en Inglés: IRS) son mediadores clave en la señalización dependiente de insulina y del factor de crecimiento semejante a insulina tipo 1 (IGF1). En ratones, la supresión de *Irs2* causa diabetes tanto en los machos como en las hembras. Las hembras son infértiles, sin embargo, el papel de IRS2 en el sistema reproductor de los machos aún no se conoce. Por ello, los objetivos del presente estudio se centraron en determinar si la ausencia de *Irs2* altera el desarrollo y función testicular. Los ratones macho adultos deficientes en *Irs2* presentan una reducción significativa en el peso y en el tamaño de los testículos. Existe una disminución significativa en el número de células de Sertoli, espermatogonias, espermatocitos y espermatozoas, sin embargo no existen diferencias en el número de células de Leydig ni se detectan cambios en la concentración plasmática de testosterona. Aparentemente, la morfología testicular no parece verse afectada. Las asociaciones celulares observadas son normales y tampoco se aprecian anormalidades en el tracto epitelial del tubo seminífero. La expresión a nivel génico y de proteína de IRS1, IRS3 e IRS4 no mostró cambios significativos en ratones deficientes en *Irs2* indicando que los otros miembros de esta familia de proteínas no compensan la pérdida de expresión de *Irs2*. La expresión del ARN mensajero del receptor de la hormona de crecimiento y la expresión proteica de SOX9 se encuentran significativamente reducidas en ratones deficientes para *Irs2*. Los ratones $Irs2^{-/-}$ presentaron mayores niveles de fosforilación de AKT, GSK3β y ERK en comparación a los silvestres pero no mostraron diferencias en la expresión de ciclina D1 o p27, proteínas relacionadas con el control del ciclo celular. En resumen, los resultados presentados en este estudio demuestran que IRS2 juega un papel crítico en la regulación del tamaño testicular. IRS2 podría modular el tamaño de los testículos al reducir o retrasar la proliferación de células de Sertoli durante el

desarrollo embrionario y/o en estadíos postnatales tempranos. Los presentes resultados proporcionan una importante base con fundamentos para entender los efectos de la señalización dependiente de IRS2 y la diabetes en la función del sistema reproductor masculino.

List of Figures

List of Tables

Abbreviations

AKT	Protein Kinase B
ANOVA	Analysis of Variance
AR	Androgen Receptor
BSA	Bovine Serum Albumin
CDK	Cyclin-Dependent Kinase
cDNA	complementary Deoxyribonucleic Acid
CNS	Central Nervous System
DAPI	4,6-diamidino-2-phenylindole dihydrochloride
DDX4	DEAD (Asp Glu Ala Asp) Box Protein 4
DNA	Deoxyribonucleic Acid
dNTP	Deoxyribonucleotide Triphosphate
DTT	Dithiothreitol
E	Embryonic day
ECad	Epithelial Cadherin
ECL	Enhanced Chemiluminescent reagent
ELISA	Enzyme-linked Immunosorbent Assay
ERK	Extracellular signal-Regulated Kinase
FSH	Follicle Stimulating Hormone
FSHR	Follicle Stimulating Hormone Receptor
GATA	Erythroid transcription factor (Globin transcription factor)
GH	Growth Hormone
GHR	Growth Hormone Receptor
GLUT4	Glucose transporter 4 (also known as SLC2A4)
GnRH	Gonadotropin Releasing Hormone
GRB2	Growth Factor Binding Protein 2
GSK3β	Glycogen Synthase Kinase 3 beta
HSD3B1	3-beta hydroxysteroid dehydrogenase
IR	Insulin Receptor
IRR	Insulin receptor-related receptor
IRS	Insulin Receptor Substrate
IGFBP	Insulin-like Growth Factor Binding Protein
IGF1	Insulin-like Growth Factor 1
IGF1R	Insulin-like Growth Factor 1 Receptor
IGF2	Insulin-like Growth Factor 2
KIT	KIT – tyrosine kinase receptor for stem cell factor (SCF)
KRLB	Kinase Regulatory-Loop Binding domain
LH	Luteinizing Hormone
LHR	Luteinizing Hormone Receptor
MAPK	Mitogen-Activated Protein Kinase
mRNA	messenger Ribonucleic Acid
mTOR	mammalian Target of Rapamycin
PBS	Phosphate Buffered Saline
PCNA	Proliferating Cell Nuclear Antigen
PCOS	Polycystic Ovary Syndrome
PCR	Polymerase Chain Reaction
PDK1	Phosphoinositide-Dependent Protein Kinase 1
PH	Pleckstrin-Homology domain
PIP_2	Phosphatidylinositol-4,5-bisphosphate

PIP_3	Phosphatidylinositol-3,4,5-triphosphate
PI3K	Phosphatidylinositol 3-Kinase
PMSF	phenylmethylsulfonyl fluoride
PTB	Phosphotyrosine-Binding domain
PVDF	Polyvinylidene fluoride
RNA	Ribonucleic Acid
SDS-PAGE	Sodium Dodecyl Sulfate - Polyacrylamide Gel Electrophoresis
SEM	Standard Error of the Mean
SH2	Src-Homology-2 domain
SOX9	Sex-determining Region of the Y chromosome – Box Containing Gene 9
SLC2A4	Glucose transporter 4 (also known as GLUT4)
SMA	Smooth Muscle Actin
SRY	Sex-determining Region of the Y chromosome
TBST	Tris-Buffered Saline with 0.5% Tween-20
TEMED	Tetramethylethylenediamine
TSC	Tuberous Sclerosis Complex

Chapter 1 Introduction

Insulin

Insulin is the most potent anabolic hormone known and is essential for appropriate tissue development, growth, and maintenance of whole-body glucose homeostasis (1) and it promotes proper metabolism, energy balance and maintenance of normal body weight (2). Insulin is secreted by the β cells of the pancreatic islets of Langerhans in response to increased circulating levels of glucose and regulates glucose homeostasis by reducing hepatic glucose output via decreased gluconeogenesis and glycogenolysis and increasing the rate of glucose uptake into muscle and adipose tissue. Insulin mRNA is translated as a single chain precursor called preproinsulin, and removal of its signal peptide during insertion into the endoplasmic reticulum generates proinsulin. Proinsulin consists of three domains: an amino-terminal B chain, a carboxy-terminal A chain and a connecting peptide in the middle called C peptide. Within the endoplasmic reticulum, proinsulin is exposed to several specific endopeptidases which excise C peptide, thereby generating the mature form of insulin. Insulin and free C peptide are packaged in the Golgi into secretory granules which accumulate in the cytoplasm. When β cells are appropriately stimulated, insulin is secreted by exocytosis and diffuses into the blood of islet capillaries. C peptide is also secreted into blood but has no known biological activity. The ultimate effector system for regulating glucose disposal is the translocation of vesicles containing glucose transporter 4 (GLUT4) to the plasma membrane to increase the rate of cellular glucose transport (3). Insulin also profoundly affects lipid metabolism, increasing lipid synthesis in liver and fat cells and attenuating fatty acid release from triglycerides in muscle and adipose tissue. Insulin resistance occurs when normal circulating concentrations of insulin are insufficient to regulate these processes appropriately. Thus, insulin resistance is a defect in signal transduction.

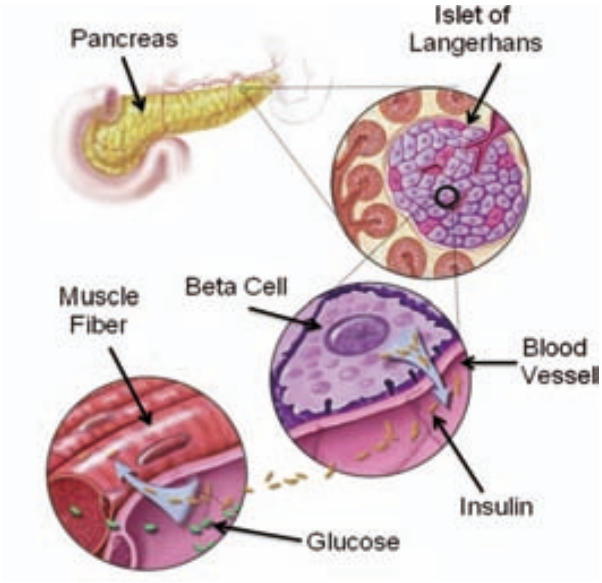

Figure 1.1. Insulin actions. Insulin is produced by pancreatic beta cells in the islets of Langerhans and regulates glucose homeostasis.

Insulin-like Growth Factor 1

Insulin-like Growth Factor 1 (IGF1) is a small polypeptide consisting of 70 amino acids with a molecular weight of 7649 Daltons (4) and is produced primarily in the liver but also by many cell types. Similar to insulin, IGF1 has an A and B chain connected by disulfide bonds and the C peptide region is composed of 12 amino acids. The structural similarity with insulin explains the ability of IGF1 to bind to the insulin receptor, albeit with lower affinity. In plasma, 99% of IGF1 is bound to a family of binding proteins (IGFBP1-6) which modulate the availability of free IGF1 to tissues (5). In humans, approximately 80% of circulating IGF1 is bound to IGFBP3, which is regulated mainly by growth hormone (GH) and slightly by IGF1 (6). IGF1 plays an important role in growth and is tightly coupled with the actions of GH and the somatotropic axis and is the mediator of the mitogenic and anabolic activity of GH (7). Laron Syndrome is a type of dwarfism in which GH resistance occurs due to mutations or deletions in the GH receptor gene and is characterized by high concentrations of GH in serum but the inability to produce IGF1 and reduced production of IGFBP3 (6).

Receptors of Insulin and IGF1

Insulin action is initiated through binding and activating its cell surface receptor, which consists of two α subunits and two β subunits that are disulfide linked into an α2β2 heterotetrameric complex (1). IGF1 signals via the type 1 IGF1 receptor (IGF1R), a widely expressed cell surface heterotetramer, highly similar to the insulin receptor (IR), which possesses intrinsic kinase activity in its cytoplasmic domains (8). Insulin binds to the extracellular α subunit of the IR/IGF1R and modifies the α subunit dimer which mediates trans-autophosphorylation between the membrane-spanning β subunits (9). This activates the intrinsic tyrosine kinase activity of the intracellular β subunit of the receptor which then leads to tyrosine phosphorylation of a variety of docking proteins. Interestingly, unlike other receptor tyrosine kinases that bind directly to the cytoplasmic tails of downstream effectors, the IR and the IGF1R utilize insulin receptor substrate (IRS) proteins to mediate the binding of intracellular effectors (10).

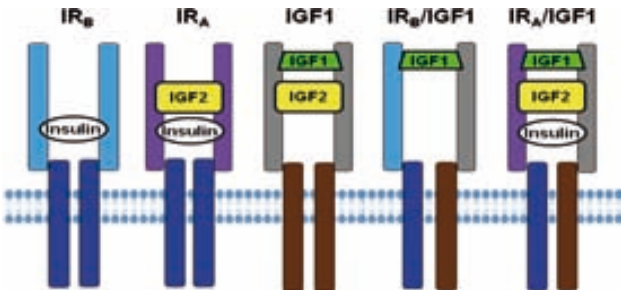

Figure 1.2. Receptors for insulin, IGF1, and IGF2. Each receptor is composed of an α2β2 heterotetrameric complex, however single αβ dimers are derived from separate genes and the IR has two splice variants, IR_B and IR_A. Therefore, combinations of the single αβ dimers exist and insulin, IGF1, and IGF2 can bind to several hybrid receptors, albeit at different affinities. The α subunit is the extracellular portion of the receptor while the β subunit spans the membrane and its cytoplasmic portion interacts with IRS proteins. The schematic shows the αβ dimers, α2β2 hybrid receptors, and the known ligands that bind each receptor.

The activity of the IR/IGF1R is tightly regulated, as unchecked activation or inactivity would lead to profound metabolic consequences. Ligand-stimulated internalization and degradation of the IR is a common feature of most insulin-resistant, hyperinsulinemic states, including obesity and type 2 diabetes (11). A third member of the insulin

receptor family is insulin receptor-related receptor (IRR). Despite similar homology, IRR is still an orphan receptor with obscure function and is expressed in few tissues (12). The main difference compared to the IR and IGF1R is the C-terminal region which lacks at least 50 amino acids (13).

Insulin Receptor Substrate Proteins

IRS proteins mediate the effects of the IR/IGF1R on cellular and whole body physiology, including reproduction (14). At least 11 intracellular substrates of the IR/IGF1R have been identified and four of these belong to the IRS family of proteins and have been named IRS1-4 (15). The IRS proteins have both pleckstrin-homology (PH) domains and phosphotyrosine-binding (PTB) domains near the N-terminus that account for the high affinity of these substrates for the IR/IGF1R.

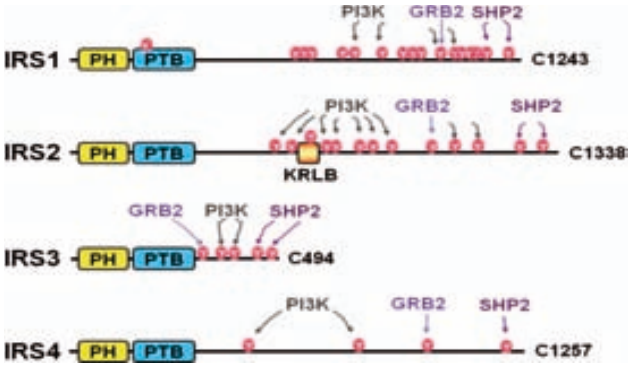

Figure 1.3. Two dimensional structure of IRS proteins. The N-terminus of IRS proteins contains pleckstrin homology (PH) and phosphotyrosine binding (PTB) domains which associate with the insulin receptor and IGF1 receptor. The center and C-terminus contain multiple potential tyrosine phosphorylation sites which then bind to other signaling molecules that contain Src-homology-2 (SH2) domains that continue to propagate the insulin/IGF1 signal. IRS2 contains a unique KRLB (Kinase Regulatory-Loop Binding) domain (aa 591-733), which serves as a negative regulatory element to control the extent of tyrosine phosphoylation of IRS2. Hence, inhibition exerted by the KRLB domain attenuates insulin signaling and action independent of serine/threonine phosphorylation (16).

The PH domain brings IRS proteins to the membrane in proximity to the IR/IGF1R and the PTB domain binds to phosphotyrosine 960 located in a NPXY (Asparagine-Proline-Unspecified-Tyrosine) motif of the juxtamembrane region of the IR/IGF1R (17), but

hindrance of these interactions by serine/threonine phosphorylation negatively affects insulin signaling (18). The center and C-terminus contain up to 20 potential tyrosine phosphorylation sites that after phosphorylation by the IR/IGF1R, bind to intracellular adaptor molecules that contain Src-homology-2 (SH2) domains, such as the p85 regulatory subunit of phosphatidylinositol 3-kinase (PI3K), or growth factor binding protein 2 (GRB2), which associates with son-of-sevenless to activate the RAS-mitogen-activated protein kinase (MAPK) pathway (15). Serine/Threonine phosphorylation adjacent to tyrosine phosphorylation sites impedes binding of the SH2 domains of IRS proteins, thus inhibiting insulin signalling (19).

Insulin Signaling

Insulin signaling is mediated by a complex, highly integrated network that controls several processes. Upon insulin binding, the IR/IGF1R phosphorylates IRS proteins which are linked to the activation of two main pathways: the PI3K-AKT pathway, which is responsible for most of the metabolic actions of insulin and the RAS-MAPK pathway which regulates expression of some genes and cooperates with the PI3K pathway to control cell growth and differentiation (15). IRS proteins are rapidly phosphorylated on their tyrosine residues following insulin binding (20), which creates recognition sites for additional effector molecules containing SH2 domains, such as GRB2 (21) and the p85 regulatory subunit of PI3K (22), thereby activating specific signaling cascades. Additionally, the IR and IGF1R can phosphorylate other substrates, such as SHC (23) and GAB1 (24), which link multiple pathways. Together, these intermediate signals stimulate a variety of different downstream biological effects including mitogenesis, gene expression, glucose transport, and glycogen synthesis.

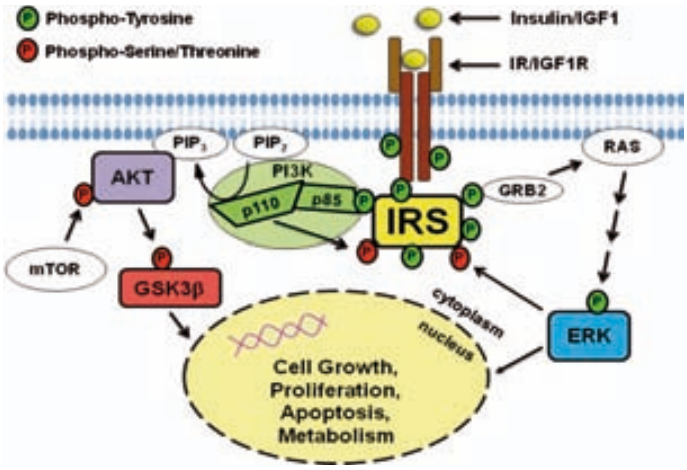

Figure 1.4. A simplified view of insulin/IGF1 signaling through IRS proteins. Activation of the IR/IGF1R by insulin/IGF1 binding, leads to autophosphorylation of the β subunits and the receptor tyrosine kinase phosphorylates IRS proteins. Phosphorylated IRS proteins recruit effector proteins such as p85 and GRB2 which bind to IRS proteins and propagate the insulin/IGF1 signal. Insulin/IGF1 signaling modulates several cellular processes such as metabolism, proliferation, cell growth, and apoptosis. See text for details.

The PI3K pathway triggers the metabolic functions of insulin. PI3K consists of a regulatory p85 and a catalytic p110 subunit. The regulatory subunit contains SH2 domains which associate with phosphorylated tyrosine residues on IRS proteins following insulin stimulation (25). The catalytic subunit then catalyzes membrane-bound phosphatidylinositol-4,5-bisphosphate (PIP_2) to phosphatidylinositol-3,4,5-triphosphate (PIP_3), which stimulates phosphoinositide-dependent protein kinase 1 (PDK1) activity. Proteins with PH domains can bind to PIP_3 and become localized to the same region, allowing for their activation. Protein kinase B (AKT) (26) and PDK1 (27) contain PH domains that bind to PIP_3 with high affinity. The binding of PIP_3 to AKT induces a conformation change that makes threonine 308 accessible to PDK1 phosphorylation (28). However, AKT is not activated until it is phosphorylated at serine 473 by the mammalian target of rapamycin (mTOR)-Rictor complex.

AKT mediates most of the PI3K-mediated metabolic actions of insulin through the phosphorylation of several substrates including other kinases, signaling proteins, and

transcription factors that affect cell growth and proliferation, cell cycle entry, and cell survival (29). Glycogen synthase kinase-3 beta (GSK3β) is a direct target of AKT and phosphorylation of serine 9 inactivates it, causing an increase in glycogen synthesis (30). GSK3β can also phosphorylate several other substrates and is involved in many processes besides the regulation of glycogen synthesis (30). Another direct target of AKT phosphorylation is tuberous sclerosis complex-2 (TSC2) which associates with TSC1 (31). TSC1/2 inhibits the growth regulator mTOR. Phosphorylation of TSC1/2 by AKT inhibits its activity and activates the mTOR pathway. mTOR associates with various proteins such as Raptor and regulates protein synthesis by phosphorylating p70 S6 kinase and eukaryotic translation initiation factor 4E binding protein 1 (31). AKT also regulates the expression of gluconeogenic and lipogenic enzymes by controlling the activity of the forkhead box class of transcription factors, which are critical for insulin action (32). Further analysis has revealed that PI3K and some of its downstream effectors are evolutionarily conserved components of the insulin signaling pathway. In *Caenorhabditis elegans*, insulin regulates metabolic activity and longevity (33) and in *Drosophila melanogaster*, insulin controls cell size (34).

The MAPK cascade is propagated by sequential phosphorylation and is an evolutionarily conserved, intracellular signal transduction pathway that responds to various extracellular stimuli and controls several fundamental cellular processes including growth, proliferation, differentiation, motility, stress response, survival, and apoptosis (35). The activation of the IR/IGF1R stimulates RAS, a small GTPase, at the plasma membrane. Activated RAS recruits RAF which then phosphorylates MEK which in turn phosphorylates extracellular signal-regulated kinase (ERK). After stimulation, ERK is able to phosphorylate hundreds of substrates in many cellular

locations and these are responsible for the induction of ERK-dependent cellular processes such as proliferation, differentiation, survival, and apoptosis (36). When deregulated, the MAPK pathway plays a major role in various pathologies such as diabetes (37).

Organization of the testis

The testis is covered by a tough fibrous capsule of connective tissue called the tunica albuginea and has two major compartments, the interstitial space and the seminiferous tubule space. The interstitial compartment contains macrophages, fibroblasts, nerve fibers, and blood and lymphatic vessels. The most abundant cell type in the interstitium is the Leydig cell, the major source of testosterone (38). Seminiferous tubules are convoluted loops that have two ends connected into the beginning of the excurrent duct system (the rete testis) by the straight tubules (tubuli recti). Although numerous convolutions are present in each loop, the tubules straighten between convolutions and travel largely in the long axis of the testis. This leads to an organized packing of tubules within the entire organ. As a result, a transverse histological section through the long axis of the testis of most species can be used to visualize cross-sectioned tubules while a histological section in the long axis of the testis will usually produce longitudinal sections (39).

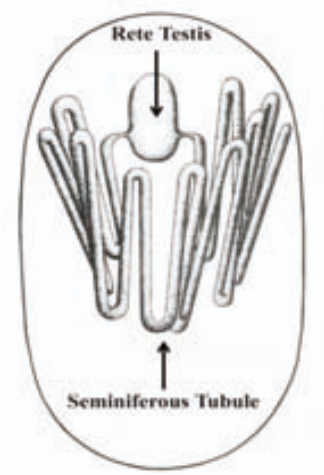

Figure 1.5. Seminiferous tubule organization in the testis. The course of one convoluted rat seminiferous tubule and its connections to the rete testis. The tubule joins the rete at both ends however it straightens along the long axis of the testis. Adapted from (39).

The seminiferous tubule compartment is bounded by the lymphatic endothelium, peritubular myoids cells, and acellular elements, which together form the lamina propria, the boundary tissue of the tubules. Basement membranes are found between the lymphatic endothelial cells and between the peritubular myoid cells and the cells within the tubules. The peritubular myoid cells are contractile and are thought to provide the major motive force for the movement of fluid and propulsion of sperm through the seminiferous tubules (40, 41). Along with the basal lamina the peritubular myoid cells provide the structural underpinning on which the Sertoli cells and basal compartment cells of the seminiferous epithelium rest. Sertoli cells provide much of the structural framework of the organization of the seminiferous epithelium.

Within the basement membrane, the seminiferous tubules are lined by a columnar epithelium composed of germ cells and the somatic Sertoli cells. Adjacent Sertoli cells are connected by tight specialized junctions to form a diffusion barrier, the blood-testis barrier, which divides the seminiferous tubule into two functional compartments, basal and adluminal. The basal compartment consists of Sertoli cells, spermatogonia, and

preleptotene-leptotene spermatocytes (42). In the adluminal compartment, primary spermatocytes divide and differentiate into germ cells in more advanced stages of spermatogenesis. Functionally, the blood-testis barrier creates a controlled microenvironment providing the nutrients, appropriate mitogens, and differentiation factors as well as an immunologically protected ambient required for the full development of germ cells (43).

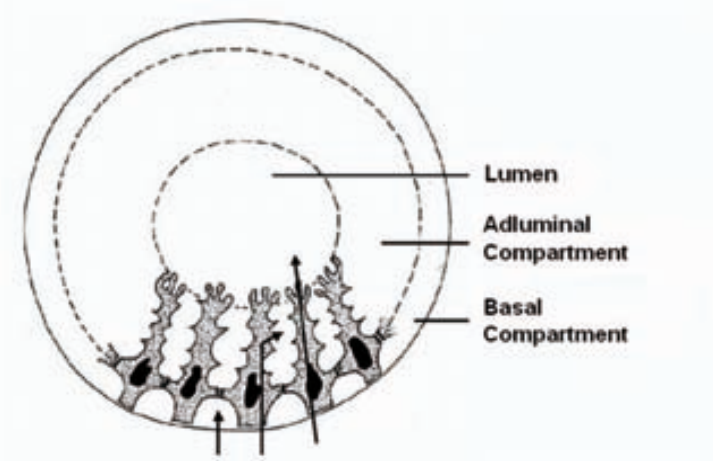

Figure 1.6. Compartments of the seminiferous tubule. Sertoli cells partition the seminiferous epithelium into a basal and adluminal compartment via Sertoli-Sertoli cell tight junctions which are the basis of the blood-testis-barrier. Arrows indicate the transport of substances to the basal compartment and to the adluminal and lumen via Sertoli cells. Adapted from (44).

Spermatogenesis

Spermatogenesis is a cyclic and highly coordinated developmental process and one of the most highly productive self-renewing systems in the body. It is complete after about 4.5 cycles which last 30-75 days in mammals (39); in mice one cycle takes approximately 38 days (45). Spermatogenesis is a continuum of cellular differentiation consisting of three major phases: spermatogonial renewal and proliferation, meiosis, and spermiogenesis. Spermatogenesis is initiated by the division of spermatogonial stem cells to form preleptotene primary spermatocytes, which undergo a final replication of nuclear DNA before entering meiotic prophase. Meiosis proceeds as primary spermatocytes develop from the preleptotene stage to leptotene, zygotene,

pachytene, and finally diplotene. The diplotene primary spermatocytes go through two meiotic divisions and give rise to round spermatids. Subsequently, round spermatids enter spermiogenesis and encounter dramatic morphological changes without a cell division to form elongated spermatids and then develop to mature spermatozoa (46).

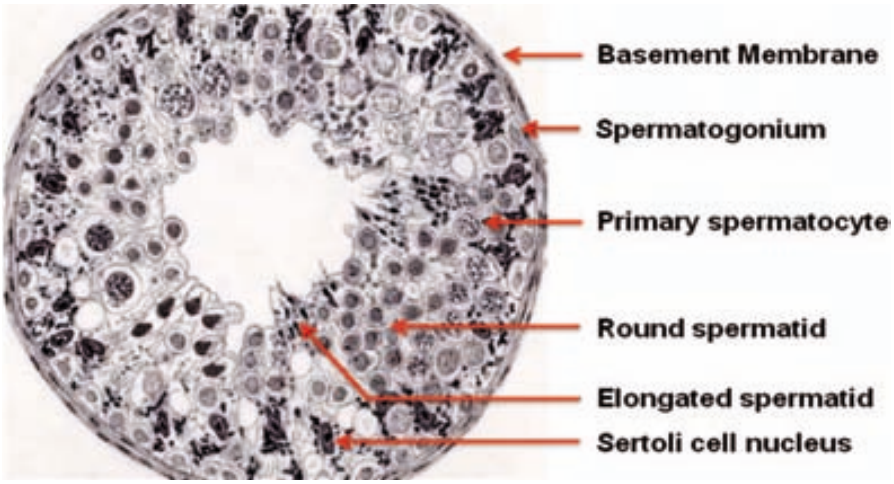

Figure 1.7. Cell types in the seminiferous tubule (diagrammatic). In mammals, sperm is generated in long, thread-like tubes, called seminiferous tubules. Each tubule is lined with an epithelium that contains spermatogonia which divide by mitosis to produce diploid spermatocytes, which then undergo meiosis to generate two haploid round spermatids, which develop further into elongated spermatids. In mammals, the entire process lasts 30-75 days. Drawing of a cross section of a seminiferous tubule at 300x from a fertile 32 yr old man. Arrows indicate cell types within the seminiferous tubule and sperm at different stages of maturation. Image adapted from (44).

This complex process is orchestrated by the expression of thousands of genes encoding proteins that play essential roles during specific phases of germ cell development. The expression of a number of these genes is developmentally regulated during spermatogenesis. Both transcriptional and translational control mechanisms are responsible for temporal and stage-specific expression patterns (47, 48). Elongated spermatids released into the lumen of the seminiferous tubules do not have the capacity to fertilize an oocyte. They acquire this ability gradually as they transit the epididymis, when they are exposed to ejaculatory fluid, and primarily during their journey in the female genital tract. Capacitation, which can be induced *in vitro* by exposing sperm to a defined medium, is a series of biochemical and physiological modifications which

render the sperm capable of fertilizing an oocyte (49), and is a key step in sperm maturation.

Sertoli cells

Sertoli cells play the lead role in development of a functional testis and are the first cells to differentiate recognizably in the indifferent fetal gonad, an event which enables seminiferous cord formation, prevention of germ cell entry into meiosis and differentiation and function of the Leydig cells (50).

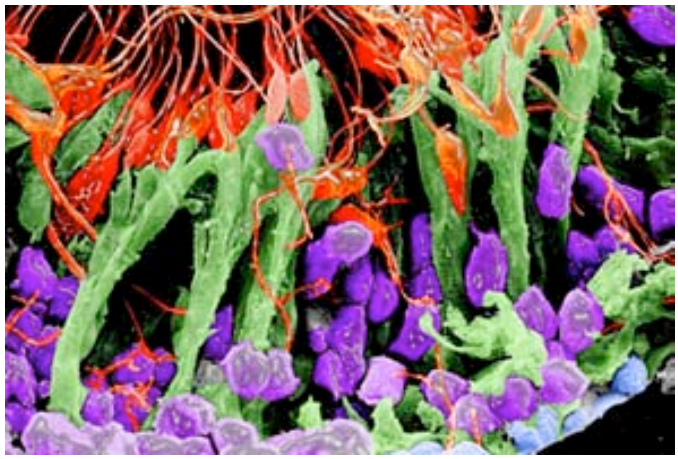

Figure 1.8. Cell types in the seminiferous tubule (electron mircograph). The seminiferous tubule contains Sertoli cells (green) embedded between differentiating spermatocytes (purple) and elongated spermatids (red). Sertoli cells nurture the developing sperm cells by secreting hormones and proteins required for spermatogenesis. Sertoli cells also establish and maintain the stem cell niche to ensure renewal of sperm cell precursors (spermatogonia, blue). Image: A seminiferous tubule from a rat imaged by scanning electron microscopy (1000x) and enhanced with color (Roger Wagner adapted from Cell 2012).

Without the physical and metabolic support of the Sertoil cells, germ cell differentiation, meiosis, and transformation into spermatozoa would not occur (51). Furthermore, the number of Sertoli cells determines the size of the testis and the number of germ cells that can be supported during spermatogenesis, thereby determining the number of sperm that can be produced (52). Differences in testis size among species and within strains are explainable by differences in the number of Sertoli cells, furthermore, testis size and sperm count in the ejaculate show a clear linear relationship in humans (51).

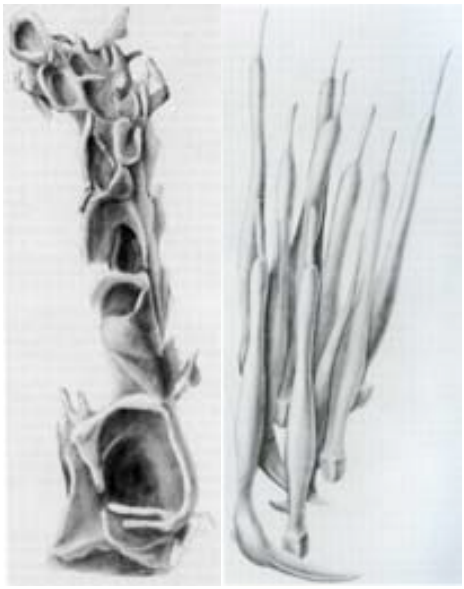

Figure 1.9. Diagram of a Sertoli cell and elongated spermatids. Left: A drawing of a reconstructed rat Sertoli cell. Overall, the cell is irregularly columnar (about 90μm high) displaying a base (below) and an apex (above). One of the lateral surfaces of the cell is shown. Numerous cup-shaped processes extend from the cell to encompass germ cells at various stages of maturation. The openings of the apical crypts where elongated spermatids attach cannot be seen from this view. Right: Ten elongated spermatids as they were seen within the apical crypts of the reconstructed rat Sertoli cell at left. On average these germ cells extend 42μm into the crypts of the Sertoli cell. The flagella of the spermatids protrude from the apex of the cell to extend into the tubular lumen. Adapted from (24).

The establishment of an adequate number of Sertoli cells at puberty is crucial for future male fertility and the number of Sertoli cells present in the adult testis depends on both the duration of the proliferative phase and the rate of division during that phase (51). In rats, Sertoli cell proliferation starts during fetal life and is complete by approximately day 16 post partum (53). Follicle stimulating hormone (FSH) signaling is a critical factor in determining the rate of Sertoli cell division (54) but other factors also have an effect on the final number of Sertoli cells (42). Thyroid hormones have been shown to be involved in determining the duration of Sertoli cell division and may be involved in the maturational changes that decrease and eliminate mitogenic responses to FSH (55).

Steroidogenesis in the Testis

Testosterone is produced by Leydig cells and binds to the androgen receptor (AR) to modulate gene transcription in target cells such as Sertoli cells (56). The development and maintenance of the male phenotype and fertility in adults are highly dependent on androgens. Testosterone controls development of the male reproductive system and secondary sex characteristics, activates the hypothalamic-pituitary-gonadal axis, masculinizes the brain, regulates sexual behavior, causes differentiation of the testis, and initiates, processes, and maintains spermatogenesis (57, 58). Postnatally, testosterone production is driven by luteinizing hormone (LH), which binds to and regulates the expression of LH receptors (LHR) on Leydig cells and maintains the local and peripheral concentration of androgens required for hormonal and reproductive development (59, 60). LHR activation also stimulates the MAPK pathway which is a critical component of Leydig cell proliferation and survival (61). The importance of MAPK signaling in Leydig cells has been demonstrated by the selective deletion of ERK1 and ERK2 which causes infertility (61).

Growth and the Somatotropic Axis

Growth in mammals is regulated by signaling pathways controlled by growth factors and hormones and is predominantly determined by more proliferation than apoptosis thereby increasing total cell number. During mouse development, this process begins in early embryogenesis at the blastocyst stage and lasts until about 4-5 months of age. GH and IGF1 exert direct and/or indirect effects on virtually every organ in the body and GH is believed to play an important role in testicular growth and development since human GH-deficiency is associated with abnormally small testes (62). Additionally, GH has been shown to directly affect steroidogenesis, spermatogenesis, and testis

differentiation as well as gonadotropin secretion and responsiveness (63, 64). GH is a major regulator of postnatal growth, although it plays a minimal role in embryonic growth in spite of growth hormone receptor (GHR) expression in embryos (65), thus, absence of GH action does not impair prenatal growth (66). IGF1 and IGF2 are part of a major growth-promoting signaling system (67), where IGF2 is essential for normal embryonic growth (68, 69), and IGF1 has continuous function throughout development (70, 71). There is considerable evidence that GH and systemic and locally produced IGF1 exert stimulatory, synergistic, or permissive effects at each level of the hypothalamic-pituitary-gonadal axis. Consistent with the multitude of actions caused by GH and IGF1, GHR and IGF1R are expressed in the brain and testes (72-74). However, the actions of IGF1 at many of these sites represent not only the actions of endocrine GH-dependent IGF1, but also those of locally derived paracrine IGF1, which may be regulated independently of GH. It is well documented that local production of IGF1 plays an important role in the intricate paracrine control of function of different types of somatic cells in the testis (75). In addition, production of both GH and IGF1 is positively related to energy intake and sexual maturation appears to be linked more closely with growth than with chronological age.

Transcriptional Regulation of Testicular Development

In mice, gonads are formed at embryonic day (E) 10.0-10.5 and consist of somatic cells and migratory primordial germ cells (76). The male phenotype is specified by the presence of the sex-determining region of the Y chromosome (SRY), which triggers differentiation of the Sertoli cell lineage, and Sertoli cells subsequently function as organizing centers and direct the differentiation of the testis. Alterations in *Sry* expression are associated with abnormal sexual differentiation and in the absence of *Sry*

XX or XY gonads do not develop testes (76-78). XY mice that are mutant for *Ir*, *Igf1r*, and *Irr* develop ovaries and exhibit a completely female phenotype and exhibit reduced expression of *Sry* and *Sox9* (SRY box containing gene 9), indicating that the insulin signaling pathway is required for male sex determination (79). In somatic cells of XY genital ridges, SRY expression starts at E10.5, peaks by E11.5 and wanes by E12.5. A few hours later SOX9 expression is upregulated to induce differentiation of Sertoli cells. SOX9 expression peaks at E11.5-12.5 and continues to be expressed in Sertoli cells postnatally and throughout adulthood (80).

Members of the globin transcription factor (GATA) family are conserved through evolution in different species and GATA1 is expressed in mouse Sertoli cells from postnatal day 7 coinciding with the first wave of spermatogenesis in prepubertal mice (81). Sertoli cells are irregularly shaped tall columnar epithelial cells and examination of cadherins in the testis has demonstrated that epithelium cadherin (ECad) is present in Sertoli cells (82). Nestin is an intermediate filament protein and is expressed in Leydig cells (83). The ATP-dependent RNA helicase DEAD (Asp Glu Ala Asp) Box Protein 4 (DDX4) is expressed in spermatocytes of all animals and is evolutionarily conserved from *Drosophila melanogaster* to mammals (84).

Proper control of the cell cycle is vital for proliferation and growth of cells, organs, and organisms. Proliferating cell nuclear antigen (PCNA) is a member of the DNA sliding clamp family which functions to provide polymerases with the high processing ability required to duplicate an entire genome. PCNA interacts with multiple proteins which are involved in metabolic pathways, DNA repair, and cell cycle regulation (85). Spermatogonia are the only cell type within the seminiferous tubules of adult mice that proliferate by mitosis and therefore PCNA is a marker of spermatogonia in the adult.

Stem cell factor is produced by Sertoli cells and binds its receptor C-KIT on spermatogonia and their interactions play an important role in the regulation of spermatogenesis and are believed to regulate germ cell proliferation, meiosis, and apoptosis (86). During development, spermatogenic cells become arrested several times. Cell cycle progression depends on the activity of a series of cyclin/cyclin-dependent kinase (CDK) complexes and cyclin D/CDK4 complexes function as master integrators that couple mitogenic signaling cascades to the cell cycle by phosphorylation and inactivation of retinoblastoma proteins, leading to dissociation of E2F transcription factors and transcriptional regulation of genes important for G1/S transition and cell cycle progression through the G1/S restriction point (87). The CDK inhibitor $p27^{kip1}$ regulates the G1/S transition and its expression is associated with inhibition of proliferation. Immunoexpression of $p27^{kip1}$ in the developing testis coincides with maturation of Sertoli cells (51).

Metabolic and Endocrine Abnormalities Impair Reproductive Function

In mammals, reproduction is controlled by the hypothalamic-pituitary-gonadal axis but is also affected by changes in energy homeostasis and metabolism. Severe dietary restriction, catabolic states, and short-term caloric deprivation impair fertility. Likewise, obesity is associated with infertile conditions such as polycystic ovary syndrome (PCOS) (88) and low sperm counts (89). PCOS is the most frequent female endocrine disorder affecting 5-10% of women and causing infertility due to dysfunctional follicular maturation and ovulation, multi-cystic ovaries, endometrial hyperplasia, and hyperandrogenemia, together with metabolic abnormalities including obesity, hyperinsulinemia, dyslipidemia, insulin resistance, an increased risk of type 2 diabetes, and cardiovascular disease (88, 90). Obesity has dramatically increased

worldwide over the past 30 years and the risk of developing chronic diseases such as diabetes mellitus, hypertension, heart disease, and stroke increase proportional to the level of obesity in both men and women (91). Obese men and women with a body mass index of more than 35kg/m^2 are 20x more likely to develop diabetes mellitus (92), which has been linked to impaired fertility in males and females (90, 93, 94).

Effects of Obesity on Spermatogenesis

An important lifestyle-dependent factor that adversely affects spermatogenesis is obesity. In Western countries, 10-30% of men are obese (95), and several studies have shown that obese men are 3x more likely to be infertile than non-obese men (95, 96). In addition, a body mass index of more than 25kg/m^2 is associated with a 25% reduction in sperm count and sperm motility (97, 98). These changes may be due to a number of factors and the alterations in sperm production may be secondary to altered hormone changes. Obesity in men is associated with reduced blood testosterone levels (99), and increased estradiol concentrations, which lead to an altered testosterone:estradiol ratio (95). The suppression of estradiol levels in obese men by aromatase inhibitors normalizes the testosterone:estradiol ratio and improves semen quality (100). However, there may be intratesticular effects that are unrelated to altered gonadotropin levels because the reduction in inhibin B levels in obese men is disproportionately larger than the change in FSH levels, suggesting that there may be direct effects of increased obesity on Sertoli cell function (95, 97, 101). Alternatively, it could indicate reduced Sertoli cell number in obese young men (101), which would be a far more serious possibility because reduced Sertoli cell number would permanently lower sperm counts, although it is unknown how or when obesity would lead to a reduction in Sertoli cell number (89). Another explanation for reduced spermatogenesis in obese men could be

deposition of fat around the scrotal blood vessels, leading to impaired blood cooling and elevated testicular temperature (102), and the sedentary lifestyle of obese men could exacerbate a temperature increase. Considering the high prevalence of obesity among young men today and the equally high prevalence of low sperm counts, it is possible that the obesity epidemic may have an impact on spermatogenesis among young men, and it may also render such individuals more susceptible to damaging effects by other lifestyle or environmental exposures.

Insulin Signaling Pathways and Reproductive Function in Females

Insulin signaling pathways regulate peripheral energy homeostasis by acting in skeletal muscle, adipose tissue, and the liver to control carbohydrate, lipid, and protein metabolism. These signals also act in other tissues, for example, in the regulation of pancreatic β cell and hypothalamic functions (103). Insulin resistance occurs when normal circulating concentrations of insulin are unable to regulate blood glucose homeostasis. Type 2 diabetes is a metabolic disorder that is characterized by high blood glucose due to insulin resistance and is closely linked to obesity. Insulin signaling has been implicated in the regulation of female reproductive function through its actions in both the central nervous system (CNS) and ovaries. Female mice that lack insulin receptors in their neurons show impaired fertility with fewer antral follicles and corpora lutea due to reduced release of LH (104). Insulin also stimulates gonadotropin releasing hormone (GnRH) secretion *in vivo*, and intracerebroventricular administration of insulin restores reproductive behavior in diabetic rats (105, 106). *In vitro* studies using immortalized GnRH neuronal cell lines have suggested that insulin regulates GnRH expression through the MAPK pathway (107). Therefore, insulin signaling in the CNS plays a role in regulating reproductive function in female rodents. Insulin signaling has

also been shown to have complex roles in ovarian function, including the regulation of ovarian steroidogenesis, follicular development, and granulosa cell proliferation (108). The strong association of insulin resistance with ovarian dysfunction in PCOS also suggests a role for insulin signaling in ovarian function (109).

Diabetes and the Role of IRS2 in Reproduction

Insulin signaling is also important in the testis and may play a critical role in testis development. Studies in rodents suggest that diabetes decreases sperm counts, and effects various aspects of male reproduction (91, 110). Interestingly, a study in men with diabetes revealed that besides a slightly reduced semen volume, conventional semen parameters such as sperm concentration, total sperm output, motility, and morphology were not different between diabetic and non-diabetic men, however there were significantly more nuclear DNA fragmentation and mitochondrial DNA deletions in sperm from diabetic patients which may impair their reproductive capability (111). *Irs2*-deficient mice develop type 2 diabetes (112). Despite the structural homology between the IRS proteins, studies in knockout mice and knockout cell lines indicate that the various IRS proteins serve complementary, rather than redundant, roles in insulin/IGF1 signaling because a deletion of each isoform has a different biological consequence (113). Mice that lack *Irs1* display profound growth retardation without a significant effect on reproduction, but diabetes does not ensue because insulin secretion increases to compensate for the mild resistance to insulin (94, 112, 114, 115). There are minimal metabolic, endocrine, and growth phenotypes upon deletion of *Irs3* or *Irs4* (14, 116, 117). However, deletion of *Irs2* leads to deregulation of the insulin signaling system, inducing insulin resistance and pancreatic β cell dysfunction manifesting in the development of type 2 diabetes (112).

Irs2-deficient females are infertile due to reduced pituitary size and gonadotroph numbers, a decrease in concentrations of LH in plasma, a reduction in ovary size, reduced numbers of follicles, and consequent anovulation (94). IRS2 signaling in the CNS plays complex roles in energy homeostasis (103), however, signaling events downstream of IRS2 in the ovary play critical roles in follicular development and ovulation by regulating key components of the cell cycle apparatus involved in the coordination of proliferation and differentiation (108).

The role of IRS2 in male reproduction is largely unknown. When $Irs2^{-/-}$ male mice were mated with $Irs2^{-/-}$ females no pregnancies were achieved (94), indicating that IRS2 plays an essential role in reproductive function. Matings between $Irs2^{+/+}$ males and $Irs2^{-/-}$ females resulted in 9% pregnancy rates (94), indicating that reproductive function is severely impaired in *Irs2*-deficient females. *Irs2*-deficient males are adequate breeders before the onset of diabetes and matings between $Irs2^{-/-}$ males and $Irs2^{+/+}$ females resulted in 88.8% pregnancy rates (94), suggesting that reproductive function is slightly reduced in *Irs2*-deficient males. However, defects in carbohydrate metabolism due to *Irs2*-deficiency are more severe in males than females, thus diabetes ensues more rapidly in males at which point they show no interest in mating (94). Although pregnancy rates of matings between various IRS genotypes indicate that *Irs2*-deficiency slightly impairs reproductive function in males, the phenotype and mechanisms are unknown.

Chapter 2 Hypothesis and Objectives

Hypothesis

The classical regulation of reproduction involves the actions of the hypothalamic-pituitary-gonadal axis. However, fertility can be modulated by the environment, lifestyle, and the availability of nutrients. In cases such as anorexia or obesity, fertility is negatively affected, demonstrating that fertility requires the integration of reproductive and metabolic signals. Mice deficient in *Irs2* develop diabetes and females are infertile. The effects of *Irs2*-deficiency on male reproduction are largely unknown. It is hypothesized that insulin/IGF1 signaling through IRS2 is required for normal testis function, growth, and development.

Objectives

1. To determine if *Irs2*-deficiency alters testicular development.
2. To characterize the testicular morphology of *Irs2*-deficient mice.
3. To determine the role of IRS2 in male reproduction.

Chapter 3 Materials and Methods

Animals

All animal experiments were performed in accordance with national regulations regarding animal welfare and were approved by the institutional committee for ethics and animal use at the Centro de Investigación Príncipe Felipe in Valencia. Mice were housed in a room with a controlled photoperiod of 12h light and 12h dark per day at 23ºC with access to food and water *Ad libitum*. *Irs2*$^{-/-}$ mice were produced and maintained on a C57Bl/6 background as described previously (112). Heterozygous *Irs2*$^{+/-}$ offspring were interbred to homozygosity and genotypes verified by semi-quantitative polymerase chain reaction (PCR). Fasting blood glucose levels were assessed by tail tip blood collection one day before tissue collection using an ELITE glucometer (Bayer Diagnostics, Barcelona, Spain), and male mice were categorized into one of three groups based on genotyping and concentrations of blood glucose: *Irs2*$^{+/+}$ (wild-type control; blood glucose 70-90mg/dl), *Irs2*$^{-/-}$ ND (non-diabetic; blood glucose 90-110 mg/dl), or *Irs2*$^{-/-}$ D (diabetic; blood glucose >250mg/dl). Unless otherwise stated, a minimum of six mice were used for each experimental group.

Blood Collection

Adult male mice were decapitated using surgical scissors. Blood was collected into a 1.5ml eppendorf tube and allowed to clot on ice before centrifuging at 13,200 x *g* for 20 min at 4^{o}C. Serum was aspirated and placed into a new 1.5ml eppendorf tube and stored at -20^{o}C until processed for quantification of testosterone by enzyme-linked immunosorbent assay (ELISA).

Tissue Collection and Processing

After decapitation, testes were immediately excised, trimmed of fat and connective tissue, and weighed using a Mettler Toledo XS105 Dual Range digital analytical balance (Barcelona, Spain). One testis was snap frozen in liquid nitrogen and stored at -80^{o}C until processed for protein or RNA extraction. The opposite testis was fixed in Bouin's Solution (Sigma, St. Louis, MO, USA) for 6hr, and then stored in 70% ethanol for 2-24hr. For paraffin embedding, Bouin's-fixed testes were placed into plastic cassettes and run through a paraffin-embedding Spin Tissue Processor machine (Myr; STP 120-2, El Vendrell, Spain) according to the following protocol: 70% ethanol for 30 min, 70% ethanol for 30 min, 96% ethanol for 30 min, 96% ethanol for 30 min, 100% ethanol for 30 min, 100% ethanol for 30 min, xylene for 10 min, xylene for 10 min, paraffin for 1hr, and paraffin for 2hr.

Sperm Capacitation

For individual mice, cauda epididymides from both testes were dissected free and rinsed in PBS before being placed in 1ml TN medium (20mM Tris (Sigma 25,285-9), 150mM NaCl (Sigma S5886) and adjusted to pH 7.4). Using scissors, the epididymides were cut several times and incubated at 37ºC, 5% CO_2 in a humidified atmosphere for 10 min to allow sperm to passively exit. Subsequently, the remaining pieces of epididymides were removed and sperm in the TN media were counted on a hemacytometer. The TN media containing sperm was transferred to a 15ml conical tube and centrifuged at 800 x *g* for 10 min at room temperature. The TN media was removed and discarded and 2ml of pre-equilibrated (overnight incubation at 37ºC, 5% CO_2 in a humidified atmosphere) of capacitation medium (100mM NaCl, 4.78mM KCl, 1.71mM $CaCl_2$-$2H_2O$, 1.19mM KH_2PO4, 1.19mM $MgSO_4$-$7H_2O$, 23.6mM sodium lactate, 0.11mg/mg sodium

pyruvate, 1mg/ml glucose, 1% penicillin/streptomycin, 0.06mg/ml phenol red, 20mM Hepes, 20mg/ml BSA, 2mg/ml $NaHCO_3$ and adjusted to pH 7.4) was carefully layered on top of the sperm pellet. This loosely-capped tube was placed in a vertical rack at 37ºC, 5% CO_2 in a humidified atmosphere for 2hr and the sperm were allowed to "swim up". The top 1ml was removed from the conical tube and sperm motility and movement patterns from *Irs2*$^{+/+}$, *Irs2*$^{-/-}$ ND, and *Irs2*$^{-/-}$ D mice were visually assessed using a microscope.

Histology and Hematoxylin and Eosin Staining

Bouin's-fixed, paraffin-embedded testes were cut using a microtome (Microm/Thermo Scientific; HM 340E, Walldorf, Germany) to a thickness of 5µm and placed on 25 x 75 x 1mm polysine slides (VWR International, Leuven, Belgium). For histology and to assess testicular architecture and structure, sections were stained with hematoxylin and eosin. Tissue sections were placed in xylene for 15 min to remove the paraffin, then hydrated in decreasing concentrations of ethanol (96% and 70%) for 5 min each, then rinsed in distilled water for 5 min. Slides were then immersed in Harris Hematoxylin solution (Sigma) for 1 min and washed in tap water for 5 min before being rinsed 10 times in 1% hydrochloric acid/70% ethanol. Tissue sections were rinsed in tap water for 5 min and subsequently stained in Eosin Y Solution (Sigma) for 10 min. After a 5 min rinse in tap water tissue sections were dehydrated in increasing concentrations of ethanol (70% and 96%) for 5 min each and finally cleared in xylene for 10 min. After a few minutes to allow the slides to dry, they were mounted using Entellan (Merck #107961, Darmstadt, Germany) and covered with a 24 x 60mm coverslip (Menzel-Glaser, Braunschweig, Germany). Images of the hematoxylin and eosin stained

testicular sections were captured using a Leica DM microscope (Switzerland) attached to Leica Application Suite (v 2.4.0 RI) imaging software.

Quantification and Analysis of Parameters of Seminiferous Tubules

Quantification of morphological measurements was performed using ImageJ software (v 1.43u, NIH, USA). The length of seminiferous tubules are packed longitudinally within the mouse testis, therefore a transverse histological section through the long axis reveals primarily round cross sections of seminiferous tubules (39). The following measurements were taken from cross sections of round seminiferous tubules. Diameters of seminiferous tubules were quantified by measuring the length of a bisecting line drawn from the basement membrane, through the center of the lumen and terminating at the basement membrane on the opposite side. The length of the seminiferous epithelium was measured by drawing a line from the basement membrane towards the lumen and measuring the linear distance of the epithelium. The circumference of the seminiferous tubules was quantified by tracing the circumference of round seminiferous tubules and measuring the distance of the line. At least 50 measurements were taken for each parameter.

Immunofluorescence

Tissue sections were placed in xylene for 15 min, then hydrated in decreasing concentrations of ethanol (96% and 70%) for 5 min each, then rinsed in distilled water for 5 min. Antigen retrieval was performed by incubating the slides in boiling (100ºC) 10mM sodium citrate buffer pH 6.0 (Sigma S1804) for 20 min. The samples were removed from the hot plate and allowed to cool in the sodium citrate buffer at room temperature for 30 min. The slides were then washed three times in distilled water for 5

min per wash and rinsed quickly in 1x phosphate buffered saline (PBS) 10 times. Non-specific binding was blocked by incubating the samples in blocking solution (1% bovine serum albumin (BSA; Sigma A7906), 5% horse serum, 0.2% Triton-X in 1x PBS, (Sigma X100)) for 1h at room temperature. The blocking solution was removed and the primary antibody of interest was added to an aliquot of blocking solution at its optimized concentration and samples were incubated overnight at 4°C. The primary antibodies used are presented in Table 3.1.

Table 3.1. Commercial Source and dilution of primary antibodies used for immunofluorescence. E-Cadherin (ECad) is a marker of Sertoli cells, Proliferating Cell Nuclear Antigen (PCNA) is a marker of spermatogonia, DEAD-box Protein 4/MVH (DDX4) is a marker of spermatocytes, Nestin is a marker of Leydig cells, and Smooth Muscle Actin (SMA) is a marker of peritubular myoid cells.

Primary Antibody	Distributor	Dilution	Conditions
ECad	Abcam ab53033 polyclonal rabbit IgG	1:100	Overnight 4ºC
PCNA	Santa Cruz sc56 monoclonal mouse IgG2a	1:100	Overnight 4ºC
DDX4	Abcam ab13840 polyclonal rabbit IgG	1:100	Overnight 4ºC
Nestin	Millipore AB5922 polyclonal rabbit IgG	1:300	Overnight 4ºC
SMA	Abcam ab5694 polyclonal rabbit IgG	1:100	Overnight 4ºC

After the incubation, the primary antibody was removed by aspiration and washed five times with 1x PBS for 5 min each. The appropriate Alexa Fluor 488 conjugated fluorescent secondary antibody (goat anti-rabbit (A11070) or goat anti-mouse (A11017) Invitrogen, Eugene, OR, USA) was added to the blocking solution at a dilution of 1:400 and incubated with the sample for 30 min at room temperature in the dark. The secondary antibody was then removed by aspiration and the sample was washed four times with 1x PBS and one time with distilled water for 5 min each. To stain nuclei, 4,6-diamidino-2-phenylindole dihydrochloride (DAPI) was diluted in 18.2 Ω MilliQ

water and 1ng/ml DAPI was incubated with all samples for 5 min at room temperature. It was removed by aspiration and washed once for 5 min in distilled water. A few drops of Dako Fluorescent Mounting Medium (Barcelona, Spain) were placed on each slide and then covered with a coverslip. The slides were sealed with nail polish to prevent dehydration and were processed immediately. Images were captured using a Leica DM 6000B fluorescent microscope attached to Leica Application Suite (v 2.8.1) imaging software.

Testis Lysis and Protein Quantification

The lysis buffer contained 50mM Tris pH 7.5, 200mM NaCl, 0.2% NP-40, and 1% Tween-20. The following components were prepared and added to the lysis buffer immediately before use, 50mM β -glycerophosphate, 2mM phenylmethylsulfonyl fluoride (PMSF), 1mM sodium orthovanadate (Na_3VO_4), and 1x Complete protease cocktail inhibitor (Roche Diagnostics, Mannheim, Germany). Each frozen testis was placed in ice-cold lysis buffer at a concentration of 100mg tissue per 1ml lysis buffer and homogenized on ice using a polytron homogenizer (PT-MR 1600E, Kinematica Inc., Littau, Switzerland). The ice-cold lysis mixture was sonicated on ice three times for 5 sec and then incubated at 4ºC for 30 min on a rotating wheel followed by centrifugation at 13,200 x *g* for 15 min. The supernatant was transferred to a new eppendorf tube and protein concentration was estimated using the BCA Protein Assay Kit (Thermo Scientific, Rockford, IL, USA) by extrapolation of known standard concentrations. Standards were prepared from 2mg/ml BSA with serial dilutions to 0.125mg/ml. Colorimetric analysis was performed in a 96-well plate using a Multiskan FC Microplate Photometer (Thermo Scientific, Finland).

Gel Preparation and SDS-PAGE

Two stacking (4.5% acrylamide) and resolving (7 or 10% acrylamide) gels were prepared the day of use according to the recipes in the table below and poured between glass plates spaced 1.5mm apart. The 7% (10%) resolving gel consisted of 7.94ml (5.93ml) of 18.2 Ω MilliQ water, 5ml (5ml) of Tris buffer pH 8.8, 4.66ml (6.67ml) acrylamide, 2ml (2ml) glycerol, 200µl (200µl) 10% ammonium persulfate, and 13.3µl (13.3µl) tetramethylethylenediamine (TEMED). The 4.5% stacking gel was made by mixing 5.4ml of 18.2 Ω MilliQ water, 2.25ml Tris buffer pH 6.8, 1.2ml acrylamide, 90µl 10% ammonium persulfate, and 6µl TEMED. First, the resolving gel was poured between the glass plates. Immediately afterwards, 70% ethanol was carefully layered on top of the resolving gel to remove bubbles and ensure a flat and even line of demarcation between the resolving and stacking gels. After the resolving gel had polymerized the ethanol was removed and the space between the glasses was blotted dry with Whatman filter paper. The stacking gel was then poured on top of the polymerized resolving gel and combs with 10 or 15 wells were set into the stacking gel to create lanes for loading protein lysates.

Laemmli 2x loading buffer, containing 4% sodium dodecyl sulphate (SDS), 10% 2-mercaptoethanol, 20% glycerol, 0.004% bromophenol blue, and 0.125M Tris-HCl and adjusted to pH 6.8, was added at a 1:1 volume to the volume of protein to be loaded in the gel. A total concentration of 20µg protein was loaded per lane and resolved under reducing and denaturing conditions by SDS-polyacrylamide gel electrophoresis (PAGE). The apparatus was set at 70V for 30min, until the leading edge had clearly passed through the stacking gel and was migrating in the resolving gel, at which time the voltage was increased to 100V and allowed to proceed for an additional 80-90 min

until the leading edge approached the end of the gel. The apparatus was turned off before the leading edge could leave the gel.

Protein Transfer and Immunoblotting

All incubation and washing steps were performed on a see-saw rocker plate. Polyvinylidene fluoride (PVDF) membranes were activated by incubating in 100% methanol for 1-2 min, and then thoroughly rinsed in distilled water and 1x tris-buffered saline with 0.5% Tween-20 (TBST) before beginning the transfer. Resolved proteins in the gel were then transferred to PVDF membranes by exposing them to an electrical current of 270mA for 1-1.5hr at 4ºC. Following transfer, PVDF membranes were washed for 5 min in 1x TBST. Non-specific binding of proteins to the PVDF membranes was blocked by incubating in blocking solution containing 1x TBST - 3% BSA for 1hr at room temperature. Primary antibodies were diluted in blocking solution and incubated according to the conditions in Table 3.2. After the incubation period the primary antibody was removed and the PVDF membrane was washed in 1x TBST five times for 5 min per wash. The appropriate horseradish peroxidase-conjugated secondary antibody (Thermo Scientific; goat anti-rabbit IgG (#31460) or goat anti-mouse IgG (#31430)) was diluted 1:10,000 in blocking solution and incubated with the PVDF membrane for 1hr at room temperature. The secondary antibody was then removed and the PVDF membrane was washed in 1x TBST five times for 5 min per wash. Reactive bands were revealed on X-ray film using Pierce Enhanced Chemiluminescent (ECL) Western Blotting Substrate reagents (Thermo Scientific #32106). Equal amounts of ECL Reagent A were mixed with Reagent B and placed on the PVDF membrane for 1-2 min. The PVDF membrane was then placed in a

Hypercassette (Amersham Biosciences, Buckinghamshire, England) and incubated with the X-ray film for the desired time to reveal bands.

Table 3.2. Commercial Source and dilution of primary antibodies used for Western blotting.

Primary Antibody	Distributor	Dilution	Conditions	MW (kD)
AKT	Cell Signaling #4691 monoclonal rabbit IgG	1:1000	Overnight 4ºC	60
p-AKT (Ser 473)	Cell Signaling #4060 monoclonal rabbit IgG	1:1000	Overnight 4ºC	60
ERK	Cell Signaling #4695 monoclonal rabbit IgG	1:1000	Overnight 4ºC	44, 42
p-ERK (Thr 202/Tyr 204)	Cell Signaling #4370 monoclonal rabbit IgG	1:1000	Overnight 4ºC	44, 42
GSK3β	Invitrogen #44610 monoclonal mouse IgG2a	1:1000	Overnight 4ºC	47
p-GSK3β (Ser 9)	Santa Cruz #11757 polyclonal rabbit IgG	1:1000	Overnight 4ºC	47
IRS1	Casero #PH polyclonal rabbit IgG	1:1000	Overnight 4ºC	180
IRS2	Santa Cruz #8299 polyclonal rabbit IgG	1:1000	Overnight 4ºC	185
IRS3	Casero #299 polyclonal rabbit IgG	1:500	Overnight 4ºC	60
IRβ	Santa Cruz #711 polyclonal rabbit IgG	1:1000	Overnight 4ºC	95
IGF1Rβ	Santa Cruz #713 polyclonal rabbit IgG	1:1000	Overnight 4ºC	97
Cyclin D1	Cell Signaling #2926 monoclonal mouse IgG2a	1:1000	Overnight 4ºC	36
p27	Santa Cruz #527 polyclonal rabbit IgG	1:1000	Overnight 4ºC	27
SOX9	Abcam ab#26414 polyclonal rabbit IgG	1:1000	Overnight 4ºC	56-60
DDX4	Abcam ab#13840 polyclonal rabbit IgG	1:1000	Overnight 4ºC	76
PCNA	Santa Cruz #56 monoclonal mouse IgG2a	1:1000	Overnight 4ºC	36
βActin	Sigma #A1978 monoclonal mouse IgG1	1:2000	1hr RT	42

Semi-quantification of immunoblotted bands

X-ray films containing the exposed bands of the protein of interest were scanned at 500 pixels and the bands were quantified using the Adobe Photoshop CS2 program. A rectangle was drawn around the band of interest and the number of pixels was quantified using the histogram tool. The same size rectangle was then moved within the same lane to an area with no bands and the pixels were quantified in this "background" area. The value of the background area was subtracted from the value of the protein of interest to yield the value of the protein of interest. For each protein of interest the same size band was used for each lane. The same procedure was used to quantify protein expression of the control protein, βActin. The value of the protein of interest was subtracted from the value of βActin to yield the value of protein expression of the protein of interest. For control mice ($Irs2^{+/+}$) the mean of the values of the protein of interest were normalized to a value of 1 arbitrary densitometric unit and the SEM was accordingly adjusted. The mean and SEM of the values from $Irs2^{-/-}$ ND and $Irs2^{-/-}$ D were compared to 1.

RNA Isolation, Template Preparation, and Generation of cDNA

All materials used for RNA isolation were RNase-free. Each frozen testis was placed into TRIzol reagent at a concentration of 100mg tissue per 1ml TRIzol and homogenized on ice using a polytron homogenizer. Total RNA was extracted according to the manufacturer's instructions (TRIzol Reagent #15596-026 Invitrogen) and resuspended in 40µl RNase-free water (Invitrogen #750024). RNA purification was achieved by treating samples with RNase-free DNase I (New England Biolabs #B0303S, Ipswich, MA, USA). The samples were then subjected to the Qiagen RNeasy Mini Kit procedure according to the manufacturer's instructions (Qiagen #74104,

Hilden, Germany). RNA concentrations were quantified using a ND-1000 Nanodrop Spectrophotometer (v3.7, Thermo Scientific, Wilmington, DE, USA) and RNA was stored at -80ºC until used for cDNA.

In 0.2ml RNase-free PCR tubes, cDNA was generated by combining 1µg RNA, 2.5ng/ml random hexamers (Invitrogen #51709), 0.5mM dNTP's (Invitrogen #10297-018), and adjusted to 12µl in RNase-free water (Invitrogen #750024), and incubated at 65ºC for 5 min then immediately transferred to 4ºC. Eight µl of the following mixture were added to each tube for a final reaction volume of 20µl: 1x RT buffer (5x First Strand Buffer (Invitrogen #494157), 10mM DTT (Invitrogen), 2U/µl RNaseOUT (Invitrogen #10777-019), 5U/µl Superscript II Reverse Transcriptase (Invitrogen), and RNase-free water (Invitrogen #750024). The tubes were briefly centrifuged and then placed on the thermocycler block (Eppendorf, Madrid, Spain) and incubated at 25ºC for 10 min, 42ºC for 50 min, 70ºC for 15 min, 4ºC ∞. When the program finished, cDNA was stored at -20ºC until used for quantitative PCR (QPCR).

Quantitative PCR

QPCR was performed using a Roche Lightcycler 480 Real-Time PCR System machine (Barcelona, Spain) with the TaqMan probes (Applied Biosystems) in Table 3.3. To prepare samples for quantitative PCR a Primer Mix and a cDNA Mix were prepared then combined for each sample in a white 96-well PCR plate. The Primer Mix consisted of 10µl Master Mix (Eurogentec #RT-QP2X-03-WOU+) and 1µl of the appropriate TaqMan Probe. The cDNA mix contained 1µl (40ng) of the appropriate cDNA and 8µl RNase-free water. Each well contained a final volume of 20µl. A piece of clear sealing tape was placed over the 96-well plate and centrifuged briefly. The

plate was then placed on the PCR machine and subjected to the following conditions: 3 min initialization at 94ºC, followed by 40 cycles of 1 min denaturation at 94ºC, 1 min annealing at 55ºC, and 1 min elongation at 72ºC. Each reaction was performed in duplicate and the value of the gene of interest was normalized to the expression of the control gene, *Gapdh*. A negative control, without a prior reverse transcription reaction, was included for each gene and data were analyzed by the comparative Ct method ($2^{-\Delta\Delta Ct}$) (118).

Table 3.3. TaqMan probes used for QPCR

TaqMan Probes	**Catalog Number**
IRS1	Mm01278327_m1
IRS2	Mm03038438_m1
IRS3	Mm00802869_g1
IRS4	Mm01340253_m1
Androgen Receptor	Mm00442688_m1
FSH Receptor	Mm00442819_m1
LH Receptor	Mm00442931_m1
IGF1 Receptor	Mm00802831_m1
GH Receptor	Mm00439093_m1
HSD3B1	Mm00476184_g1
SLC2A4	Mm00436615_m1
DDX4	Mm00802445_m1
GATA1	Mm01352636_m1
KIT	Mm00445212_m1
GAPDH	Mm99999915_g1

Quantification of Testosterone

An enzyme-linked immunosorbent assay (ELISA; USCN Life Science, Wuhan, China) was used to determine the concentration of testosterone in mouse serum according to the manufacturer's instructions. A volume of 50µl serum was analyzed per mouse. Each sample was analyzed in duplicate and values were extrapolated from a standard curve prepared with known concentrations of testosterone.

Statistical Analysis

Statistical analyses were performed using GraphPad Prism (v4.0). All data are presented as mean ± SEM. The differences in means were analyzed by ANOVA or unpaired t-test followed by Tukey's Multiple Comparsion Test or Welch's Correction, respectively. A difference of $P<0.05$ was considered statistically significant.

Chapter 4 Results

Deletion of *Irs2* causes reduced testis size and weight

Consistent with published results, many *Irs2*$^{-/-}$ mice in these studies were diabetic (D) by 10-12 weeks after birth. To avoid this additional complication in the analysis of IRS2 function in testicular development, we carefully monitored mice to permit an experimental group which had not yet developed hyperglycemia (ND). Testes from *Irs2*$^{-/-}$ mice were reduced in size and weight but no differences in body weight were observed compared to *Irs2*$^{+/+}$ mice. When testes weights were normalized to body weights, the ratio of testes:body weights was significantly reduced in *Irs2*$^{-/-}$ mice. There were no differences in testes weight between *Irs2*$^{-/-}$ ND and *Irs2*$^{-/-}$ D mice (Table 4.1).

Table 4.1. Glucose concentrations, body weight, and testes weight in *Irs2*-deficient mice. *Irs2*$^{-/-}$ male mice exhibited extremely elevated glucose levels by 10-12 weeks after birth indicative of hyperglycemia and were thus considered diabetic. However, glucose concentrations from 6-week old *Irs2*$^{-/-}$ mice were comparable to those of *Irs2*$^{+/+}$ mice. Body weights did not differ between groups but testes weight and therefore the testes:body weight ratio was reduced in *Irs2*-deficient mice. Results are mean ± SEM of 10 mice per measurement per phenotype. Values within columns with an asterisk are significantly different than *Irs2*$^{+/+}$; ** denotes $P<0.01$ and *** denotes $P<0.001$. ND=non-diabetic, D=diabetic.

Genotype	Glucose (mg/dl)	Body Weight (g)	Testes Weight (mg)	Testes:Body Weight
Irs2$^{+/+}$	80.7 ± 1.1	21.9 ± 0.6	200.0 ± 8.1	9.4 ± 0.3
Irs2$^{-/-}$ ND	104.5 ± 3.9	20.0 ± 0.8	107.5 ± 3.3***	5.3 ± 0.2 ***
Irs2$^{-/-}$ D	278.9 ± 18.0**	21.5 ± 0.8	113.1 ± 2.7***	5.2 ± 0.2 ***

To determine if there were differences in testis structure and morphology, testicular cross sections were examined. Histological examination of the testis by hematoxylin and eosin staining demonstrated that there were no apparent alterations in the seminiferous epithelium or interstitial space. The seminiferous epithelium contained Sertoli cells and germ cells at all stages of differentiation and in apparently normal cellular associations (Figure 4.1). However, the diameter of the seminiferous tubules

(Figure 4.2A), the length of the seminiferous epithelium (Figure 4.2B), and the circumference of the seminiferous tubules (Figure 4.2C) were significantly reduced in *Irs2*$^{-/-}$ mice.

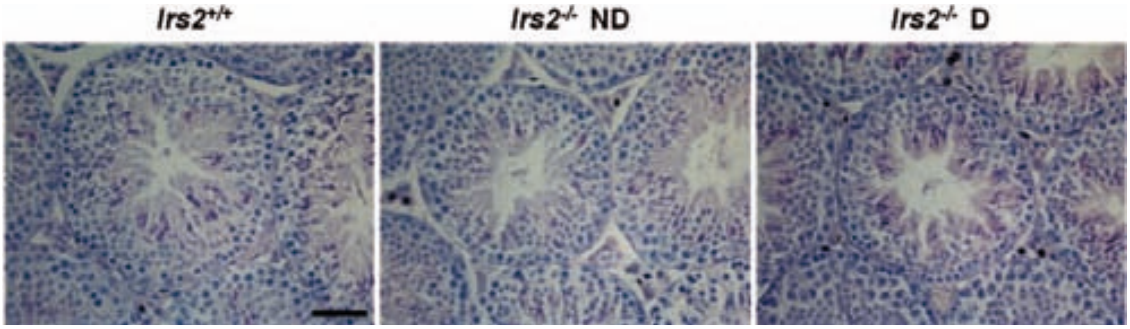

Figure 4.1. Histology of testicular cross sections. Testes were Bouin's-fixed paraffin-embedded and 5µm transverse histological sections were cut through the long axis of the testis. Hematoxylin and eosin staining of testicular cross sections demonstrates that spermatogenesis appears to proceed normally in the absence of *Irs2* with normal cellular associations in the seminiferous epithelium and numerous spermatozoa in the lumen. There are no morphological abnormalities in the interstitial space. Representative images were captured using a 40x objective. The scale bar represents 50µm.

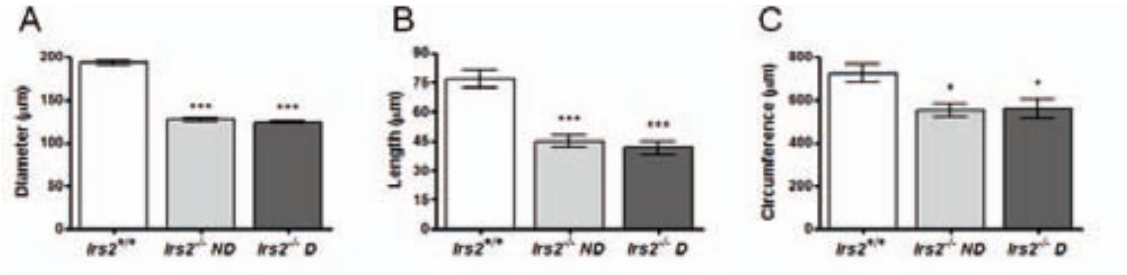

Figure 4.2. Morphological measurements of seminiferous tubules. The diameter of the seminiferous tubule (A), the length of the seminiferous epithelium (B), and the circumference of the seminiferous tubule (C), were measured from hematoxylin and eosin stained testicular cross sections using the ImageJ software program. Results for each measurement are mean ± SEM from a minimum of 50 randomly selected seminiferous tubules from transverse histological sections through the long axis of the testis from five mice from each phenotype. Asterisks denote a significant difference compared to *Irs2*$^{+/+}$; * $P<0.05$, *** $P<0.001$.

Testes weight is reduced in *Irs2*$^{-/-}$ neonatal mice

To determine if the reduced testis phenotype of *Irs2*-deficient adult mice occurs as an embryonic defect, testes from neonatal mice were analyzed at postnatal day 0 (day of birth), postnatal day 2, and postnatal day 4. Testes weight (Figure 4.3C) but not seminiferous tubule diameter (Figure 4.3D) of *Irs2*$^{-/-}$ mice at postnatal day 0 was

significantly reduced compared to *Irs2*$^{+/+}$ mice. At postnatal day 2 there were no differences in testes weight or seminiferous tubule diameter (Figure 4.4). At postnatal day 4 testes weight (Figure 4.5C) was significantly reduced but there were no differences in the diameter of seminiferous tubules (Figure 4.5D).

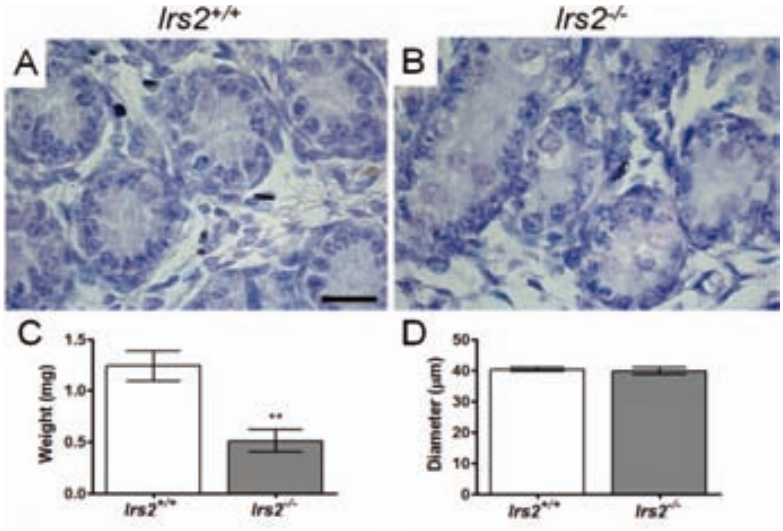

Figure 4.3. Histology and morphological measurements of neonatal testes at postnatal day 0 (day of birth). Testes from (A) *Irs2*$^{+/+}$ mice and (B) *Irs2*$^{-/-}$ mice were fixed in Bouin's solution and embedded in paraffin, and sections were cut to a thickness of 5µm and stained with hematoxylin and eosin. Images were captured at 100x magnification under oil immersion, scale bar represents 20µm. Representative images from 7 *Irs2*$^{+/+}$ mice and 3 *Irs2*$^{-/-}$ mice. (C) Testes weight at postnatal day 0. Testes were dissected free from surrounding tissue and weighed. Results are mean ± SEM of 5 mice per genotype. (D) Seminiferous tubule diameter at postnatal day 0. The diameter of seminiferous tubules was measured using ImageJ software. Results are mean ± SEM of at least 50 seminiferous tubules from 5 mice per genotype. Asterisks above bars denote a significant difference compared to *Irs2*$^{+/+}$; ** $P<0.01$.

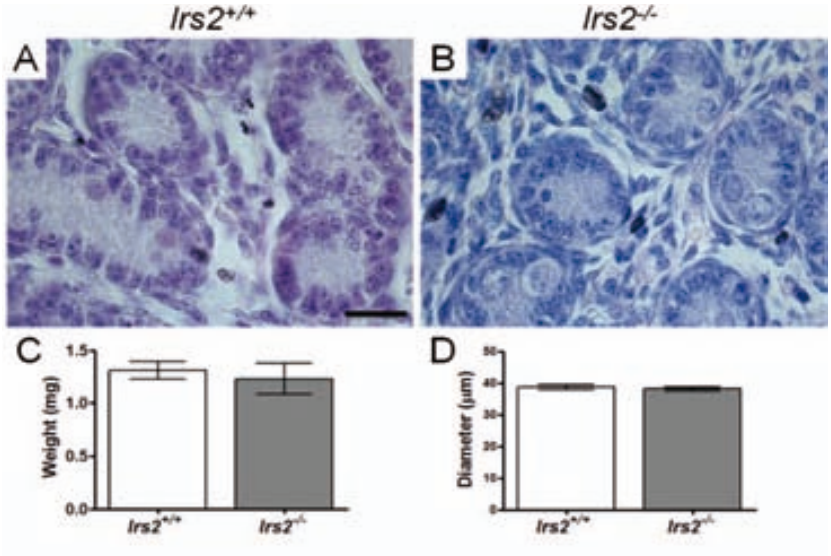

Figure 4.4. Histology and morphological measurements of neonatal testes at postnatal day 2. Testes from (A) *Irs2*$^{+/+}$ mice and (B) *Irs2*$^{-/-}$ mice were fixed in Bouin's solution and embedded in paraffin, and sections were cut to a thickness of 5µm and stained with hematoxylin and eosin. Images were captured at 100x magnification under oil immersion, scale bar represents 20µm. Representative images from 6 *Irs2*$^{+/+}$ mice and 3 *Irs2*$^{-/-}$ mice. (C) Testes weight at postnatal day 2. Testes were dissected free from surrounding tissue and weighed. Results are mean ± SEM of 13 *Irs2*$^{+/+}$ mice and 3 *Irs2*$^{-/-}$ mice. (D) Seminiferous tubule diameter at postnatal day 2. The diameter of seminiferous tubules was measured using ImageJ software. Results are mean ± SEM of at least 50 seminiferous tubules from 6 *Irs2*$^{+/+}$ mice and 3 *Irs2*$^{-/-}$ mice.

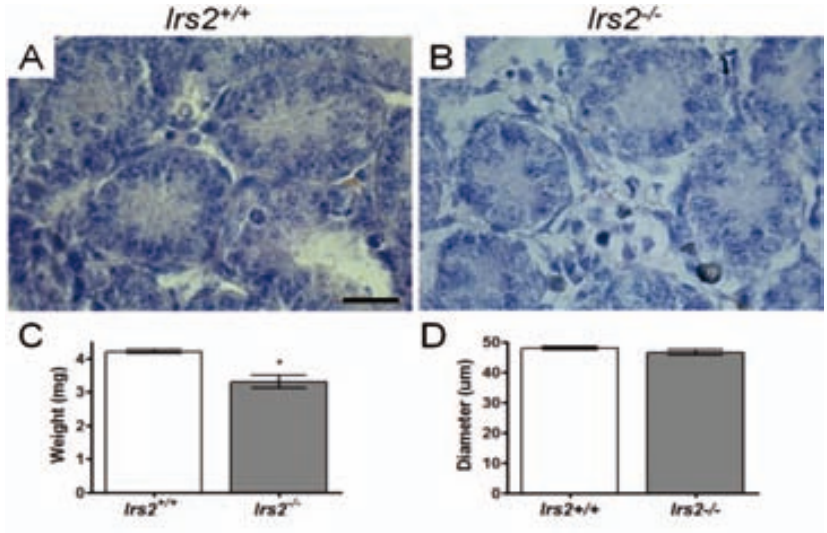

Figure 4.5. Histology and morphological measurements of neonatal testes at postnatal day 4. Testes from (A) *Irs2*$^{+/+}$ mice and (B) *Irs2*$^{-/-}$ mice were fixed in Bouin's solution and embedded in paraffin, and sections were cut to a thickness of 5µm and stained with hematoxylin and eosin. Images were captured at 100x magnification under oil immersion, scale bar represents 20µm. Representative images are from 3 mice from each genotype. (C) Testes weight at postnatal day 4. Testes were dissected free from surrounding tissue and weighed. Results are mean ± SEM of 3 mice from each genotype. (D) Seminiferous tubule diameter at postnatal day 4. The diameter of seminiferous tubules was measured using ImageJ software. Results are mean ± SEM of at least 50 seminiferous tubules from 7 *Irs2*$^{+/+}$ mice and 3 *Irs2*$^{-/-}$ mice. Asterisks denote a significant difference compared to *Irs2*$^{+/+}$; * $P<0.05$.

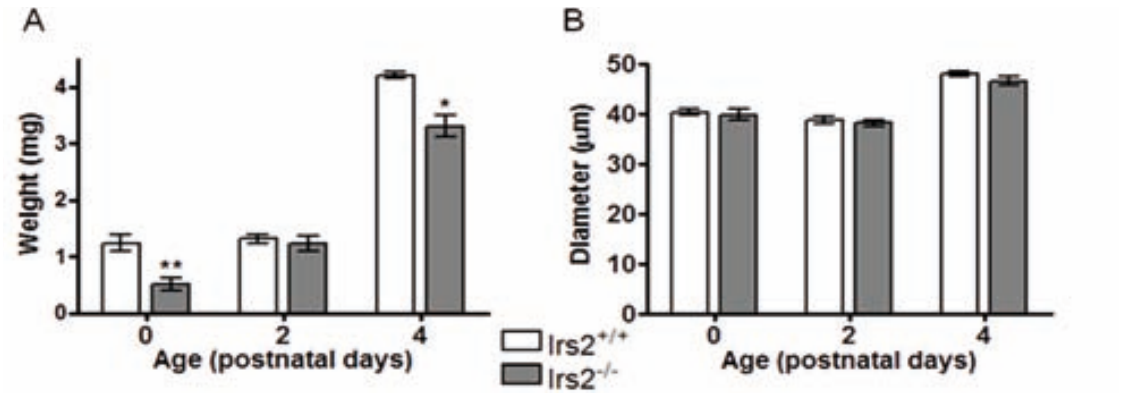

Figure 4.6. Testes weight and seminiferous tubule diameter in neonatal mice. (A) Testes weights in *Irs2*$^{-/-}$ mice were significantly reduced at postnatal day 0 and 4 but not at postnatal day 2. (B) There were no differences in seminiferous tubule diameter between *Irs2*$^{+/+}$ or *Irs2*$^{-/-}$ mice at postnatal day 0, 2, or 4. Asterisks denote a significant difference compared to *Irs2*$^{+/+}$; * P<0.05, ** P<0.01.

Irs2-deficiency causes reduced testicular cell number and sperm counts

As germ cells mature during spermatogenesis, they are in constant contact with Sertoli cells in the seminiferous epithelium. To determine if reduced testis size was associated with reduced cell number and ultimately sperm production, multiple cell types were assessed. Significantly fewer Sertoli cells, spermatogonia, and spermatocytes per cross section of seminiferous tubule were detected in *Irs2-/-* mice compared to *Irs2*$^{+/+}$ mice. (Figure 4.7A-C). Interestingly, there were no differences in the number of Leydig cells per interstitial space between *Irs2*$^{+/+}$, *Irs2*$^{-/-}$ ND, or *Irs2*$^{-/-}$ D mice (Figure 4.7D). Consistent with the reduction in spermatogonia and spermatocytes, there were significantly fewer spermatozoa in the epididymides of *Irs2*$^{-/-}$ mice (Figure 4.7E). However, after *in vitro* capacitation, spermatozoa from all mice appeared normal with no abnormal movement patterns and motility was indistinguishable between *Irs2*$^{+/+}$ and *Irs2*$^{-/-}$ mice. Although differences in cell number between the *Irs2*$^{+/+}$ and *Irs2*$^{-/-}$ mice were observed, there were no significant differences in cell number in any cell type between the *Irs2*$^{-/-}$ ND and *Irs2*$^{-/-}$ D mice (P>0.05) (Figures 4.7A-E).

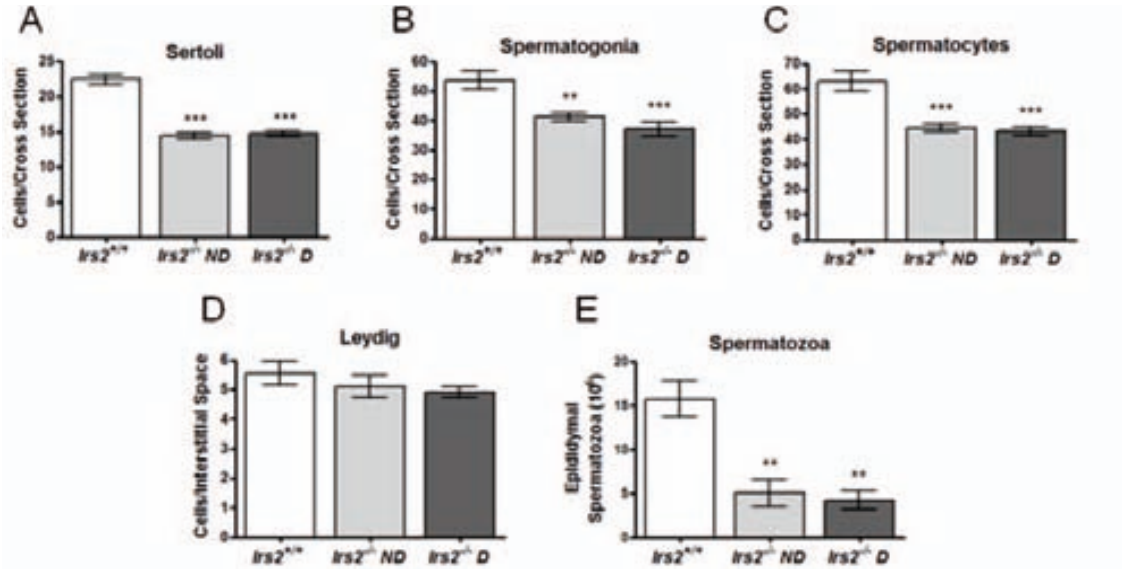

Figure 4.7. Analysis of distinct cell populations in the testis and epididymis. (A-D) Transverse histological sections 5µm in thickness were cut through the long axis of Bouin's-fixed paraffin-embedded testes and sections were probed with antibodies to specific cell types which were visualized and quantified by immunofluorescence. (A-C) Cell number per cross section of seminiferous tubule was quantified in a minimum of 50 seminiferous tubules per mouse. (A) Sertoli cells were immunostained with an antibody to ECad. Results are mean ± SEM of 7 *Irs2*$^{+/+}$, 12 *Irs2*$^{-/-}$ ND, and 11 *Irs2*$^{-/-}$ D mice. (B) Spermatogonia were immunostained with an antibody to PCNA. Results are mean ± SEM of 10 *Irs2*$^{+/+}$, 11 *Irs2*$^{-/-}$ ND, and 10 *Irs2*$^{-/-}$ D mice. (C) Spermatocytes were immunostained with an antibody to DDX4. Results are mean ± SEM of 7 *Irs2*$^{+/+}$, 8 *Irs2*$^{-/-}$ ND, and 7 *Irs2*$^{-/-}$ D mice. (D) Leydig cells were immunostained with an antibody to Nestin. A minimum of 50 interstitial spaces per mouse were examined. Results are mean ± SEM of 5 mice per phenotype. (E) The epididymides from each mouse were dissected free from the testes, placed in medium, and repeatedly sliced open to allow spermatozoa to be released. Spermatozoa were collected and counted on a hemacytometer. Results are mean ± SEM of 5 *Irs2*$^{+/+}$, 4 *Irs2*$^{-/-}$ ND, and 4 *Irs2*$^{-/-}$ D mice. Asterisks denote a significant difference compared to *Irs2*$^{+/+}$; ** $P<0.01$, *** $P<0.001$.

Irs2-deficient mice have reduced cell number but normal cell density

To determine if the difference in cell number of specific cell types within the testis was attributable to the difference in testis size, cell number was normalized. For cells within the seminiferous tubule, cell number was normalized to the diameter of the seminiferous tubule. There were no differences in the number of Sertoli cells, spermatogonia, or spermatocytes per micrometer of diameter of seminiferous tubules between phentoypes (Figure 4.8A-C). However, because there were more interstitial spaces per equivalent area, when the number of Leydig cells was normalized per mm^2 of testis tissue, there

were significantly more Leydig cells in testes of *Irs2*$^{-/-}$ mice (Figure 4.8D). The number of epididymal spermatozoa was normalized to weight of testis tissue (mg) and there were no significant differences in the number of spermatozoa that were produced by *Irs2*$^{+/+}$, *Irs2*$^{-/-}$ ND, or *Irs2*$^{-/-}$ D mice (Figure 4.8E). Thus, the testes of *Irs2*$^{-/-}$ mice were smaller and contained fewer cells than those of *Irs2*$^{+/+}$ mice but the morphology and function appeared normal.

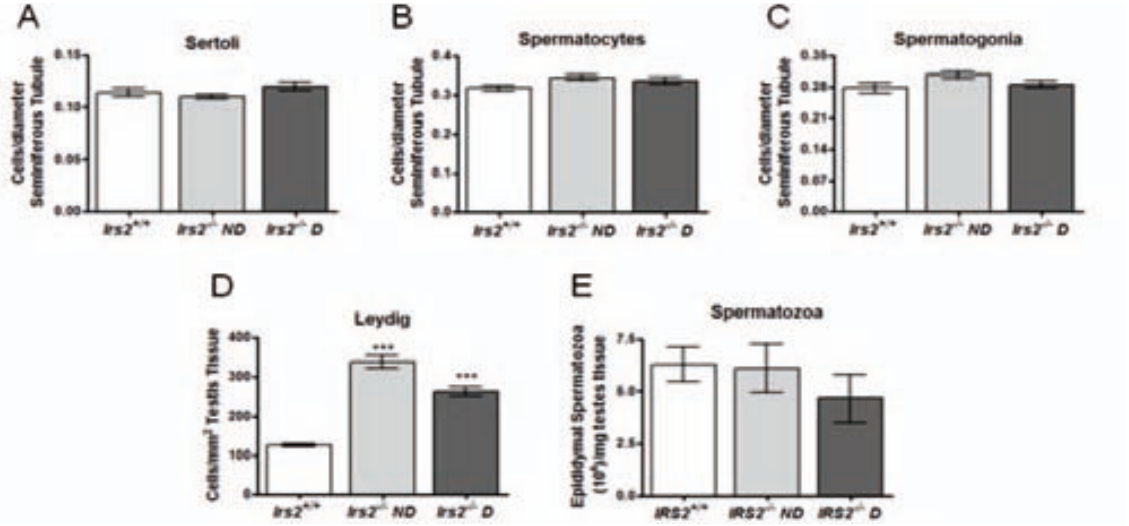

Figure 4.8. Cell density in the testis. (A-C) For cells within the seminiferous tubule, cell number was normalized to the diameter of the seminiferous tubule. Results are mean ± SEM of 5 mice from each phenotype. (D) The number of Leydig cells was normalized to mm^2 of testis tissue. Results are mean ± SEM of 5 mice from each phenotype. (E) The number of spermatozoa collected from epididymides was normalized to weight of the testes. Results are mean ± SEM of 7 *Irs2*$^{+/+}$, 3 *Irs2*$^{-/-}$ ND, and 5 *Irs2*$^{-/-}$ D mice. Asterisks denote a significant difference compared to *Irs2*$^{+/+}$; *** P<0.001.

The basement membrane is intact in *Irs2-/-* mice

The integrity of the basement membrane and the surrounding peritubular myoid cells were examined to determine if the decline in the number of cells in the testis of *Irs2*$^{-/-}$ mice was due to a disruption of the basement membrane. Staining patterns of peritubular myoid cells with an antibody against smooth muscle actin were similar in *Irs2*$^{+/+}$ and *Irs2*$^{-/-}$ mice (Figure 4.9). In addition, there were no differences in staining patterns of collagen IV or smooth muscle actin (Figure 4.10).

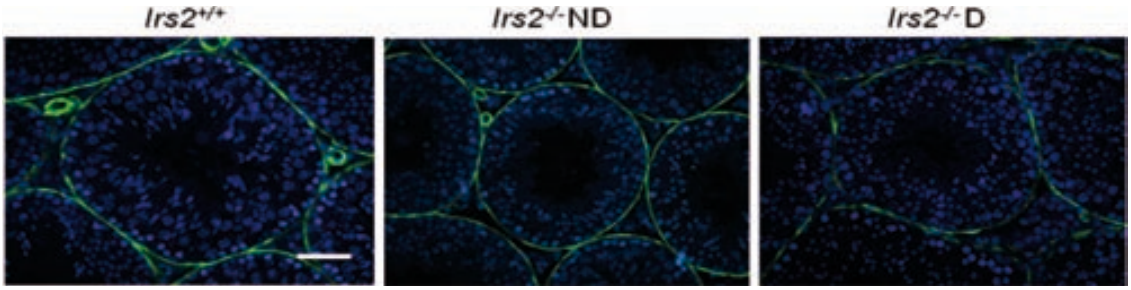

Figure 4.9. Analysis of protein markers of peritubular myoid cells. Representative immunofluorescent localization of peritubular myoid cells using an anti-smooth muscle actin antibody. Representative images from testicular cross sections from each phenotype are shown. All images were captured using a 40x objective and the scale bar represents 50µm. Nuclei were counterstained with DAPI.

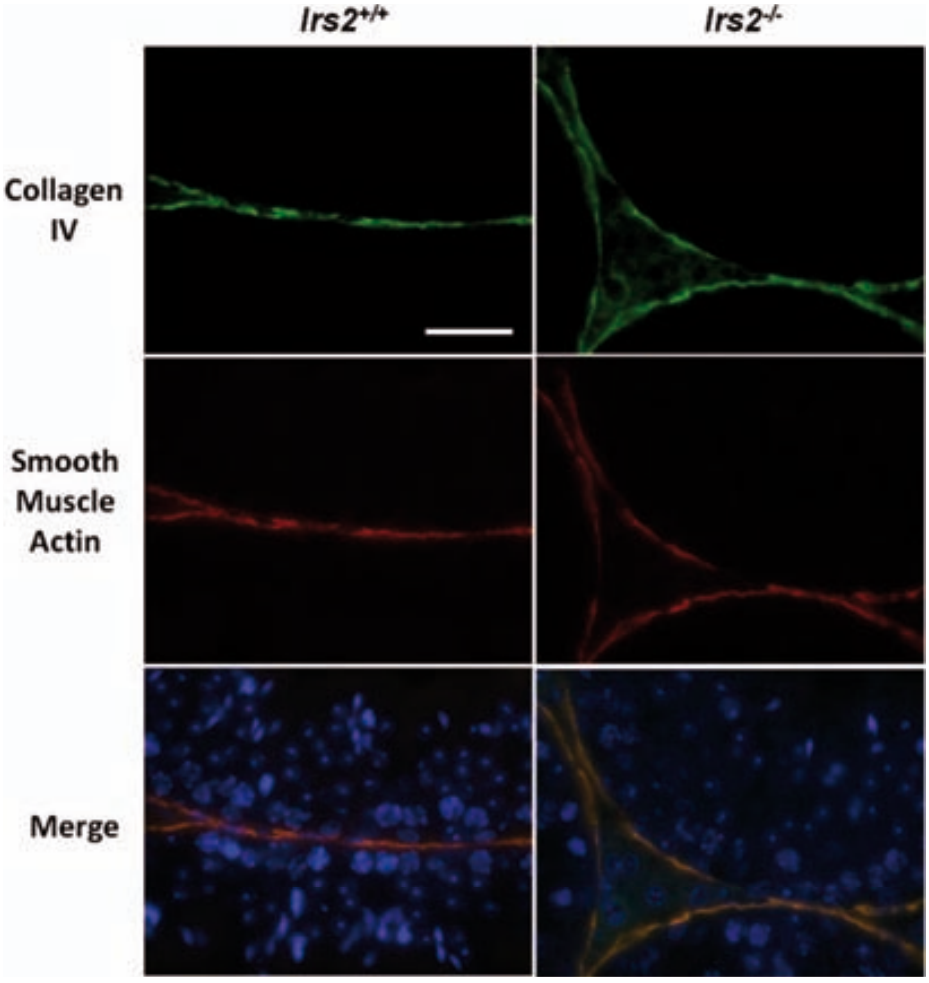

Figure 4.10. Analysis of protein markers of the basement membrane. Immunofluorescent localization of collagen using an anti-collagen IV antibody (green) and peritubular myoid cells using an anti-smooth muscle actin antibody (red). Representative images from testicular cross sections from *Irs2*$^{+/+}$ and *Irs2*$^{-/-}$ mice are shown. Nuclei in the merged image were labelled with DAPI. All images were captured using a 100x objective under oil immersion and the scale bar represents 20µm.

Gene expression of cell markers in the testis does not change in *Irs2*-deficient mice

Quantitative PCR was performed to analyze gene expression of various markers in the testis. Relative gene expression of transcription factor and Sertoli cell marker *Gata1* (51) (Figure 4.11A), spermatogonial stem cell marker *Kit* (Figure 4.11B), and spermatocyte cell marker *Ddx4* (Figure 4.11C) was unchanged between phenotypes. Testosterone exhibits its biological effects by binding to the androgen receptor which is localized to Sertoli and peritubular myoid cells (119). The enzyme 3β-hydroxysteroid dehydrogenase (HSD3B1) converts 5-Androstene-3β, 17β-diol to testosterone and is localized to Leydig cells. Gene expression of *Androgen receptor* (Figure 4.11D) and *Hsd3b1* (Figure 4.11E) revealed that there were no differences between $Irs2^{+/+}$, $Irs2^{-/-}$ ND, or $Irs2^{-/-}$ D mice.

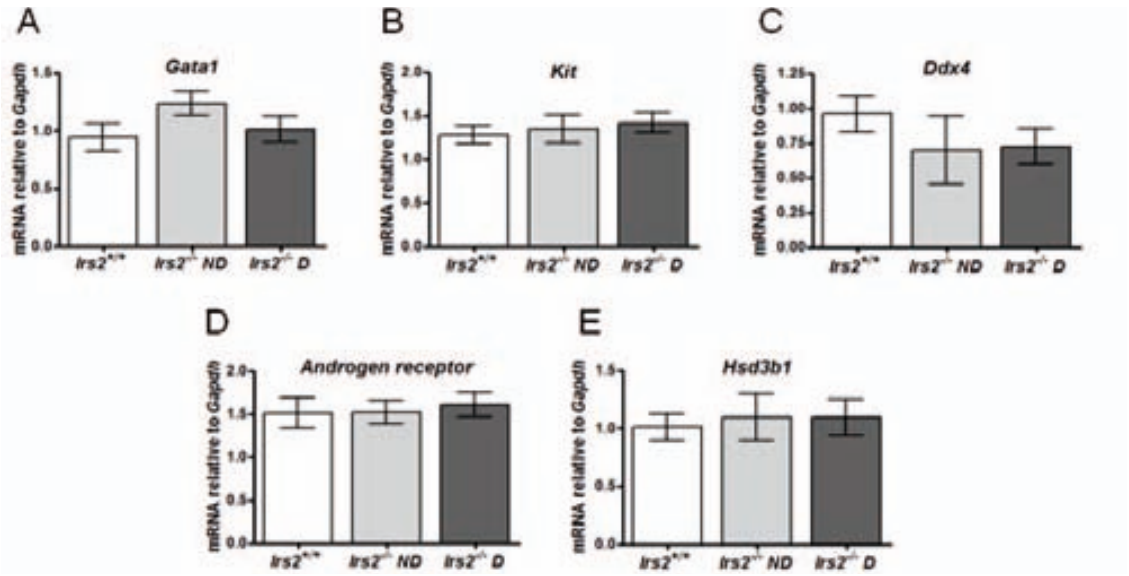

Figure 4.11. Gene expression of testicular markers. Testes were lysed and total RNA was isolated, cDNA was generated, and QPCR was performed using TaqMan probes. Each reaction was performed in duplicate and the value of the gene of interest was normalized to the expression of a control gene, *Gapdh*. A negative control, without a prior reverse transcription reaction, was included for each gene and data were analyzed by the comparative Ct method ($2^{-\Delta\Delta Ct}$) (118). For each gene, results are mean ± SEM of 7 $Irs2^{+/+}$, 7 $Irs2^{-/-}$ ND, and 6 $Irs2^{-/-}$ D mice. Relative gene expression of Sertoli cell marker *Gata1* (A), spermatogonial cell marker *Kit* (B), spermatocyte cell marker *Ddx4* (C), *Androgen receptor* (D) which is localized to Sertoli and peritubular myoid cells, and Leydig cell marker *Hsd3b1* (E).

***Irs2*-deficiency causes differences in protein expression of testicular markers**

Sertoli cell nuclei were localized by immunofluorescence using an anti-ECad antibody (Figure 4.12A). Semi-quantification of band intensity of Sertoli cells by immunoblotting using an anti-SOX9 antibody demonstrated that there was significantly reduced expression of Sertoli cells in *Irs2*-deficient mice (Figure 4.12B-C). Spermatogonia were localized by immunofluorescence using an anti-PCNA antibody (Figure 4.13A) and semi-quantification of band intensity from immunoblots demonstrated that there was a significant increase in protein expression of spermatogonia in the testes of adult *Irs2*-deficient mice (Figure 4.13B-C). Spermatocytes were localized by immunofluorescence using an anti-DDX4 antibody (Figure 4.14A) and semi-quantification of band intensity from immunoblots demonstrated that there were no changes in protein expression of DDX4 in the testes of *Irs2*-deficient mice (Figure 4.14B-C). Leydig cells were localized to the interstitial space and visualized by immunofluorescence using an anti-Nestin antibody (Figure 4.15).

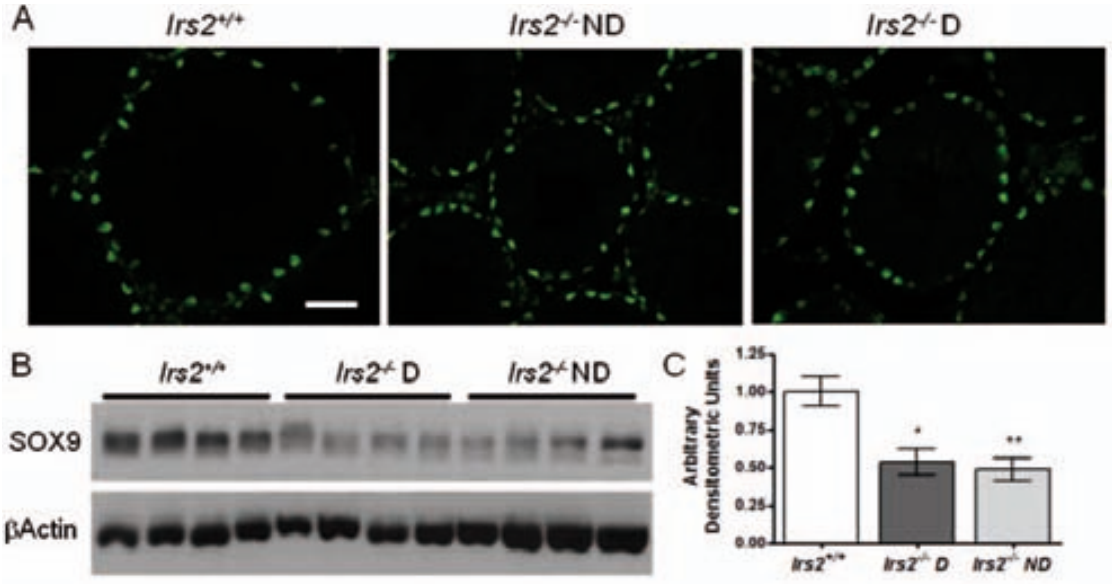

Figure 4.12. Protein analysis of Sertoli cell markers. A) Immunofluorescent localization of Sertoli cell nuclei using an anti-ECad antibody. Representative images from testicular cross sections from each phenotype are shown. All images were captured using a 40x objective and the scale bar represents 50µm. B) Immunoblot of testes lysates. A total of 20µg of testis lysate was loaded per lane and probed with an anti-SOX9 antibody. βActin was used as a loading control. Results are from 4 mice per phenotype. C) Band intensities were quantified using Adobe Photoshop (v.CS2) and the intensity ratio of SOX9/βActin is shown. Values for $Irs2^{+/+}$ were set as 1 arbitrary densitometric unit. Asterisks denote a significant difference compared to $Irs2^{+/+}$; * P<0.05, ** P<0.01.

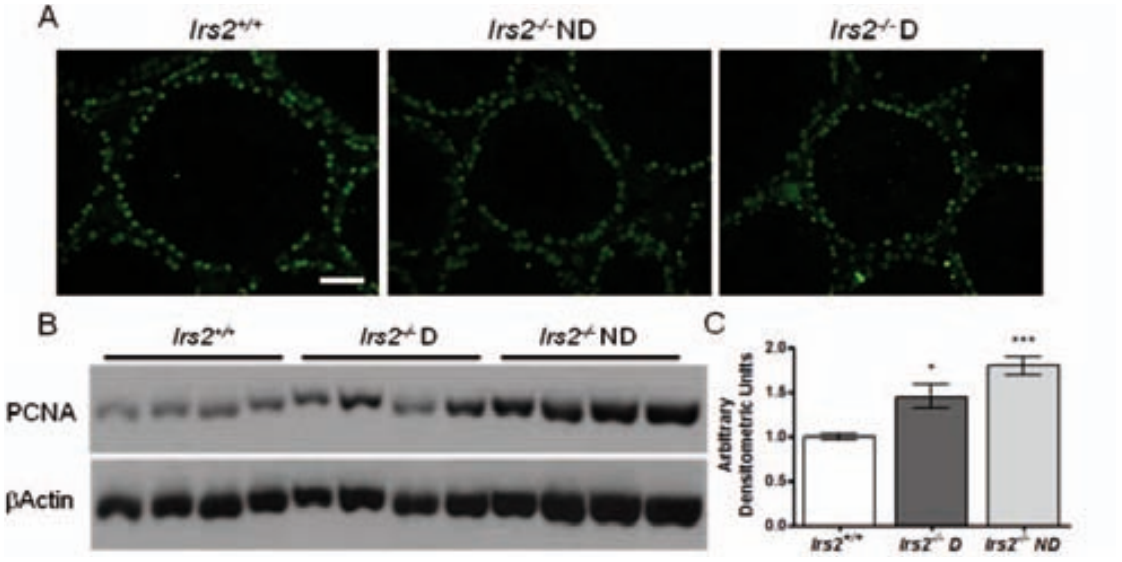

Figure 4.13. Analysis of PCNA expression as a marker of spermatogonia. A) Immunofluorescent localization of spermatogonial cell nuclei using an anti-PCNA antibody. Representative images from testicular cross sections from each phenotype are shown. All images were captured using a 40x objective and the scale bar represents 50µm. B) Immunoblot of testes lysates. A total of 20µg of testis lysate was loaded per lane and probed with an anti-PCNA antibody. βActin was used as a loading control. Results are from 4 mice per phenotype. C) Band intensities were quantified using Adobe Photoshop (v.CS2) and the intensity ratio of PCNA/βActin is shown. Values for $Irs2^{+/+}$ were set as 1 arbitrary densitometric unit. Asterisks denote a significant difference compared to $Irs2^{+/+}$; * P<0.05, *** P<0.001.

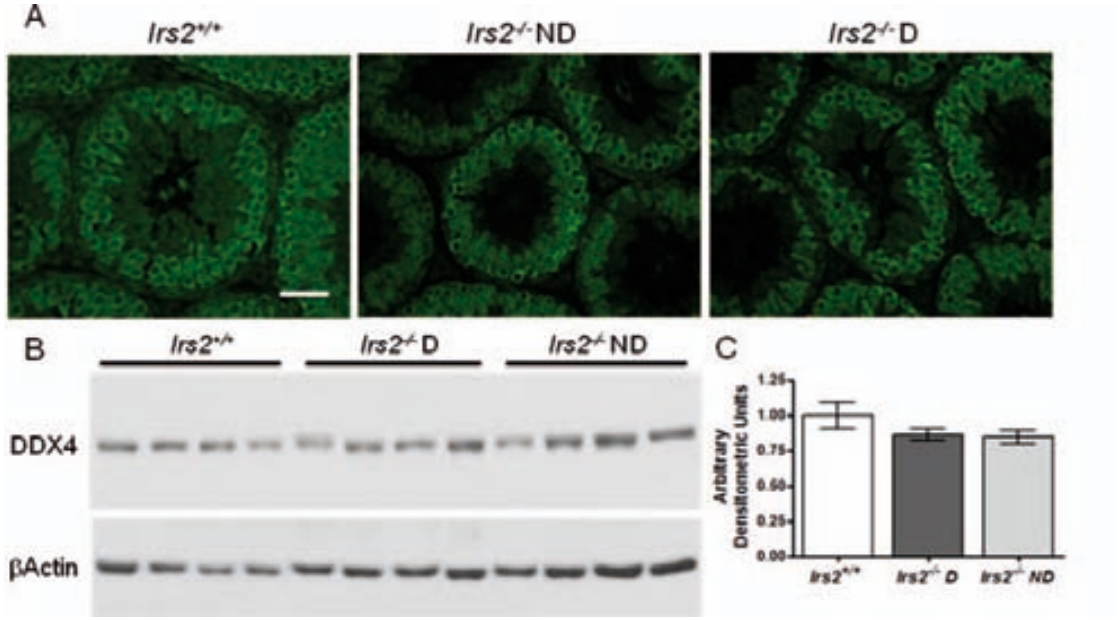

Figure 4.14. Analysis of DDX4 as a marker of spermatocytes. A) Immunofluorescent localization of spermatocytes using an anti-DDX4 antibody. Representative images from testicular cross sections from each phenotype are shown. All images were captured using a 40x objective and the scale bar represents 50µm. B) Immunoblot of testes lysates. A total of 20µg of testis lysate was loaded per lane and probed with an anti-DDX4 antibody. βActin was used as a loading control. Results are from 4 mice per phenotype. C) Band intensities were quantified using Adobe Photoshop (v.CS2) and the intensity ratio of DDX4/βActin is shown. Values for $Irs2^{+/+}$ were set as 1 arbitrary densitometric unit.

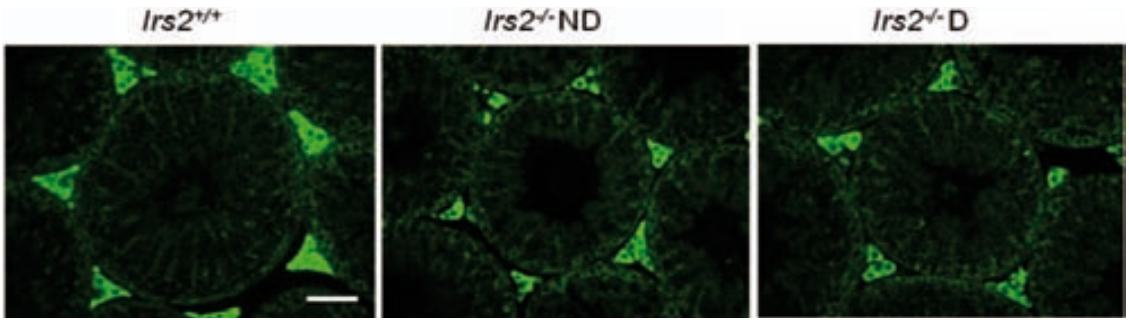

Figure 4.15. Analysis of protein markers of Leydig cells. Immunofluorescent localization of Leydig cells using an anti-Nestin antibody. Representative images from testicular cross sections from each phenotype are shown. All images were captured using a 40x objective and the scale bar represents 50µm.

Expression of IRS proteins does not change in the testes of *Irs2*-deficient mice

There were no changes in gene expression of *Irs1*, *Irs3*, or *Irs4* between $Irs2^{+/+}$ and $Irs2^{-/-}$ mice (Figure 4.16). To determine if there were changes in protein expression of IRS proteins, immunoblotting was performed. Consistent with the lack of difference in gene expression of the IRS proteins, there were no significant changes in protein expression of IRS1 (Figure 4.17) or IRS3 (Figure 4.19) in $Irs2^{-/-}$ mice compared to $Irs2^{+/+}$ mice. As expected there was no protein expression of IRS2 (Figure 4.18) in $Irs2^{-/-}$ mice.

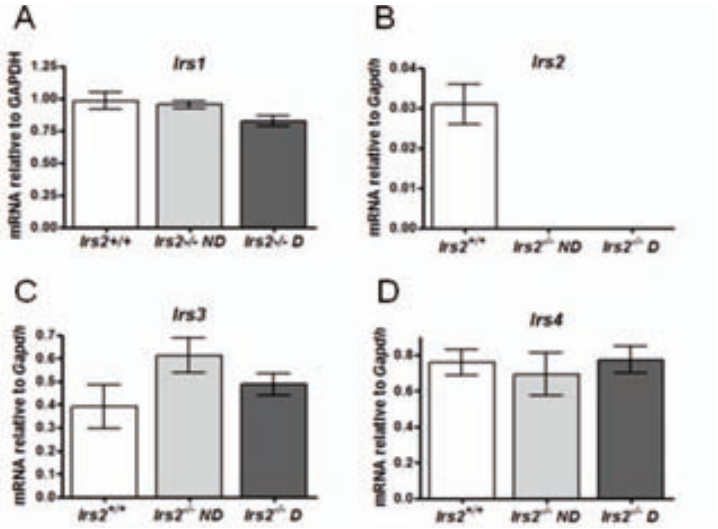

Figure 4.16. Gene expression of IRS proteins in the testis. Testes were lysed and total RNA was isolated, cDNA was generated, and QPCR was performed using TaqMan probes. Each reaction was performed in duplicate and the value of the gene of interest was normalized to the expression of a control gene, *Gapdh*. A negative control, without a prior reverse transcription reaction, was included for each gene and data were analyzed by the comparative Ct method ($2^{-\Delta\Delta Ct}$) (118). For each gene, results are mean ± SEM of 5 $Irs2^{+/+}$, 5 $Irs2^{-/-}$ ND, and 6 $Irs2^{-/-}$ D mice.

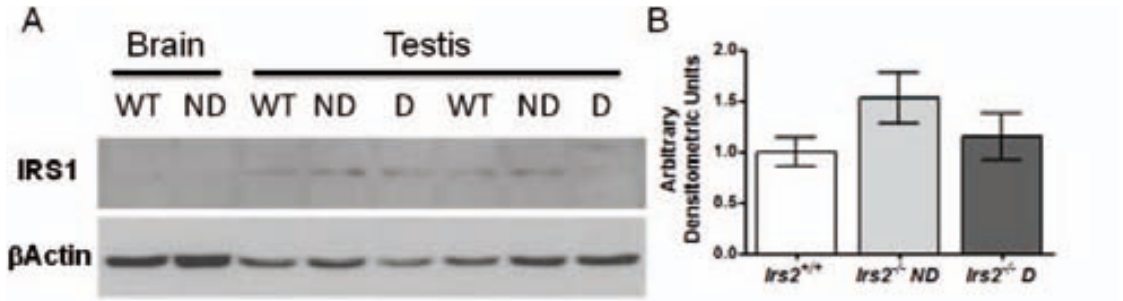

Figure 4.17. Representative immunoblots of IRS1 in the testis. A) Testes were lysed, 80µg of total protein was loaded per lane, and blots were probed with an anti-IRS1 antibody. βActin was used as a loading control. WT = *Irs2*$^{+/+}$, ND = *Irs2*$^{-/-}$ ND, and D = *Irs2*$^{-/-}$ D. B) Band intensities were quantified using Adobe Photoshop (v.CS2) and the intensity ratio of IRS1/βActin is shown. Values for *Irs2*$^{+/+}$ were set as 1 arbitrary densitometric unit. Densitometric values are mean ± SEM of 4 mice per phenotype.

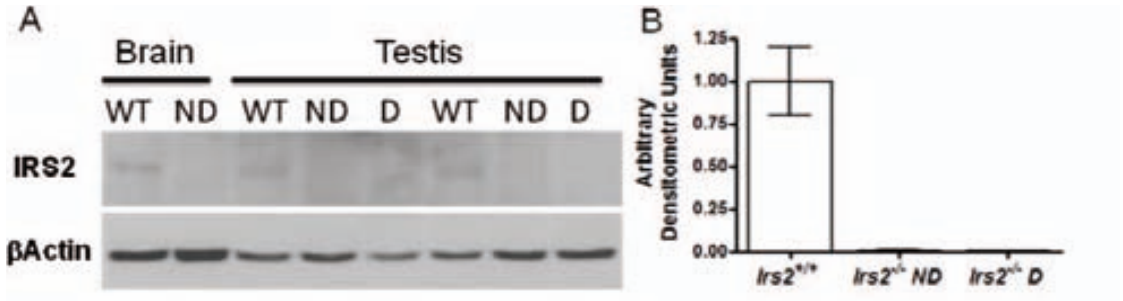

Figure 4.18. Representative immunoblots of IRS2 in the testis. A) Testes were lysed, 80µg of total protein was loaded per lane, and blots were probed with an anti-IRS2 antibody. βActin was used as a loading control. WT = *Irs2*$^{+/+}$, ND = *Irs2*$^{-/-}$ ND, and D = *Irs2*$^{-/-}$ D. B) Band intensities were quantified using Adobe Photoshop (v.CS2) and the intensity ratio of IRS2/βActin is shown. Values for *Irs2*$^{+/+}$ were set as 1 arbitrary densitometric unit. Densitometric values are mean ± SEM of 4 mice per phenotype.

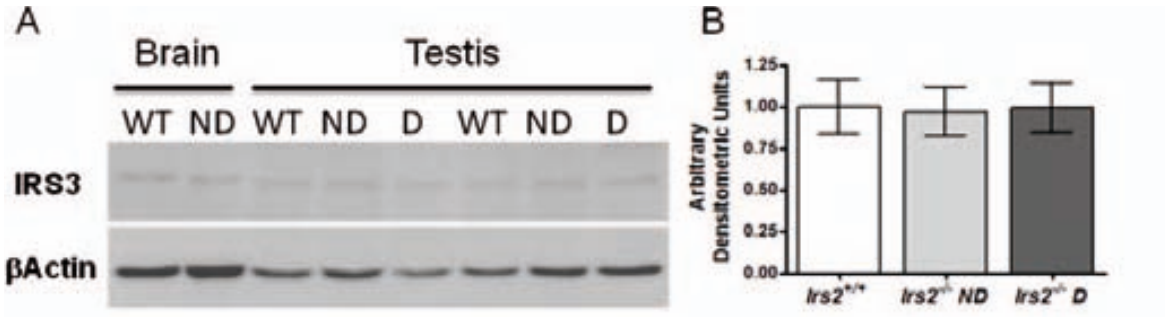

Figure 4.19. Representative immunoblots of IRS3 in the testis. A) Testes were lysed, 80µg of total protein was loaded per lane, and blots were probed with an anti-IRS3 antibody. βActin was used as a loading control. WT = *Irs2*$^{+/+}$, ND = *Irs2*$^{-/-}$ ND, and D = *Irs2*$^{-/-}$ D. B) Band intensities were quantified using Adobe Photoshop (v.CS2) and the intensity ratio of IRS3/βActin is shown. Values for *Irs2*$^{+/+}$ were set as 1 arbitrary densitometric unit. Densitometric values are mean ± SEM of 4 mice per phenotype.

Endocrine-related markers are differentially expressed in testes of normoglycemic *Irs2*$^{-/-}$ mice

The testis of *Irs2*$^{-/-}$ ND mice showed a significant increase in the expression of genes for insulin-like growth factor 1 receptor (*Igf1r*), glucose transporter 4 (*Slc2a4*), luteinizing hormone receptor (*Lhr*), and follicle stimulating hormone receptor (*Fshr*), but when diabetes ensued, the expression of these genes declined to levels comparable to *Irs2*$^{+/+}$ mice (Figure 4.20). There was a significant reduction in gene expression of growth hormone receptor (*Ghr*) in the testes of *Irs2*$^{-/-}$ ND and *Irs2*$^{-/-}$ D mice (Figure 4.20).

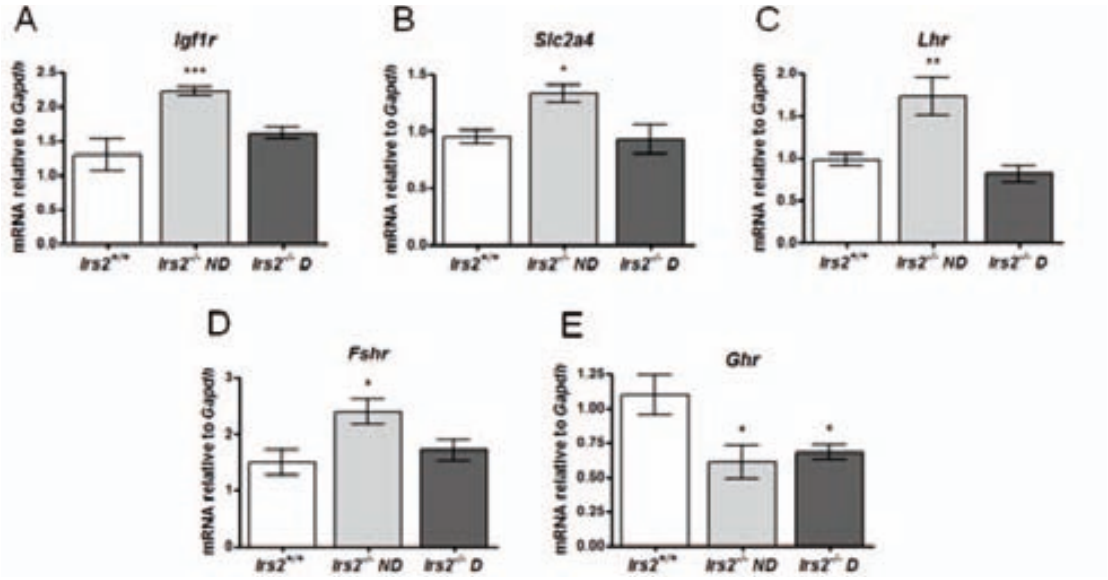

Figure 4.20. Gene expression of endocrine-related markers in the testis. Testes were lysed and total RNA was isolated, cDNA was generated, and QPCR was performed using TaqMan probes. Each reaction was performed in duplicate and the value of the gene of interest was normalized to the expression of a control gene, *Gapdh*. A negative control, without a prior reverse transcription reaction, was included for each gene and data were analyzed by the comparative Ct method ($2^{-\Delta\Delta Ct}$) (118). For each gene, results are mean ± SEM of 6 mice per phenotype. Relative gene expression of *Igf1r* (A), *Slc2a4* (B), *Lhr* (C), *Fshr* (D), and *Ghr* (E). Asterisks denote a significant difference compared to *Irs2*$^{+/+}$; * $P<0.05$, ** $P<0.01$, *** $P<0.001$.

Increased protein expression of IGF1Rβ but not IRβ in *Irs2*-deficient mice

Results from QPCR suggested that *Igf1r* was increased in testes of $Irs2^{-/-}$ mice and this was confirmed by immunoblot analysis (Figure 4.21A, C). However protein expression of IRβ was not significantly altered in *Irs2*-deficient mice (Figure 4.21B, D).

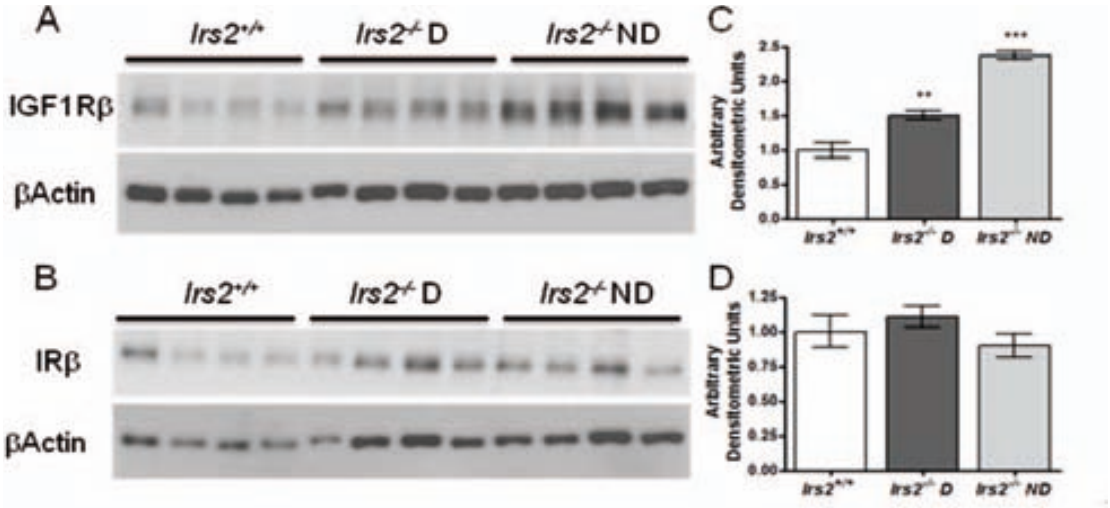

Figure 4.21. Representative immunoblots of IGF1Rβ and IRβ in the testis. Testes were lysed, 20μg of total protein was loaded per lane, and blots were probed with an antibody against IGF1Rβ (A) or IRβ (B). βActin was used as a loading control. Band intensities were quantified using Adobe Photoshop (v.CS2) and the intensity ratio of IGF1Rβ/βActin (C) and IRβ/βActin (D) is shown. Values for $Irs2^{+/+}$ were set as 1 arbitrary densitometric unit. Results are mean ± SEM of 4 mice per phenotype. Asterisks denote a significant difference compared to $Irs2^{+/+}$; ** P<0.01, *** P<0.001.

Increased phosphorylation of proteins in the MAPK and PI3K pathways in testes of *Irs2*-deficient adult mice

To determine whether the absence of *Irs2* alters insulin-mediated signal transduction in the testis, various pathways were assessed. Testes from adult mice were homogenized and protein levels of key components in the PI3K and MAPK pathways were analyzed by immunoblotting. There were no differences in the expression of AKT, ERK, or GSK3β between $Irs2^{+/+}$ and $Irs2^{-/-}$ mice (Figures 4.22A, 4.23A, and 4.24A, respectively), however, there was a significant increase in basal phosphorylation of AKT, ERK, and GSK3β in the testes of *Irs2*-deficient mice compared to $Irs2^{+/+}$ mice (Figures 4.22B, 4.23B, and 4.24B, respectively). Additionally, expression of cell cycle

regulators was studied. Interestingly, there were no changes in protein expression of cyclin D or p27 (Figure 4.25).

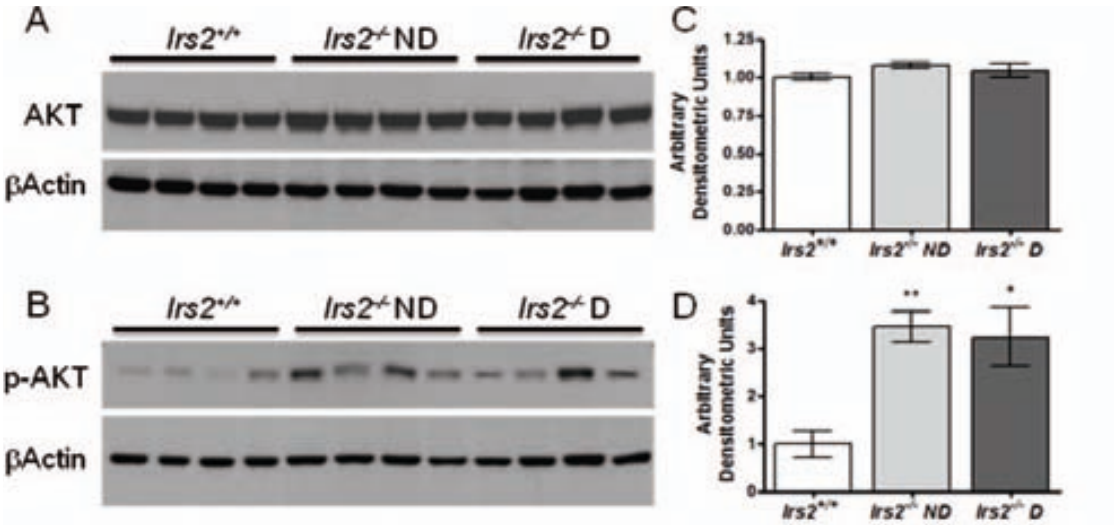

Figure 4.22. Representative immunoblots of AKT and p-AKT in the testis. Testes were lysed, 20µg of total protein was loaded per lane, and blots were probed with an antibody against AKT (A) or p-AKT (B). βActin was used as a loading control. Band intensities were quantified using Adobe Photoshop (v.CS2) and the intensity ratio of AKT/βActin (A) and p-AKT/βActin (B) is shown. Values for $Irs2^{+/+}$ were set as 1 arbitrary densitometric unit. Results are mean ± SEM of 4 mice per phenotype. Asterisks denote a significant difference compared to $Irs2^{+/+}$; * P<0.05, ** P<0.01.

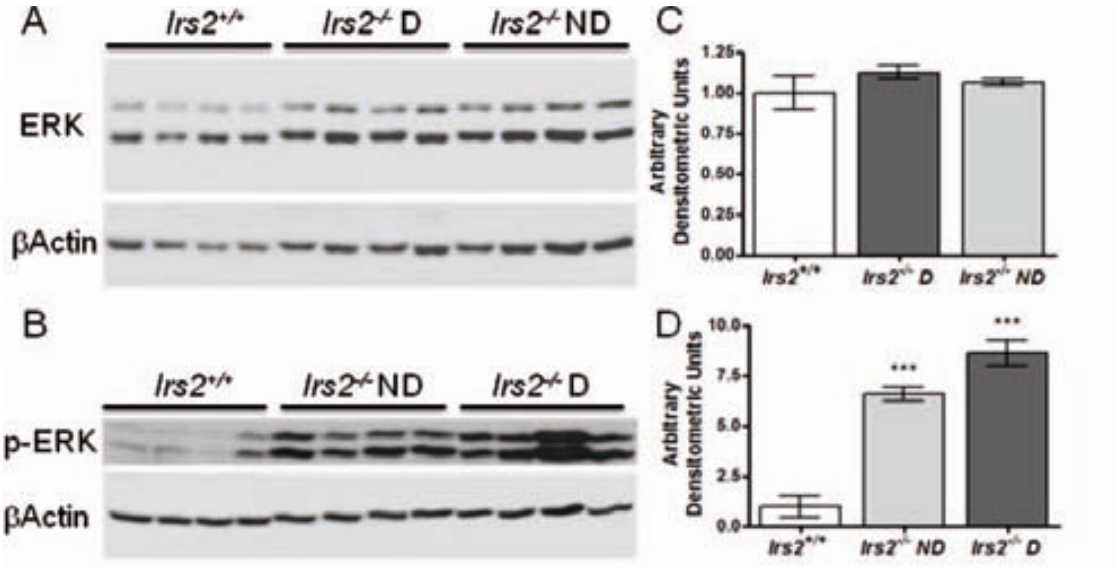

Figure 4.23. Representative immunoblots of ERK and p-ERK in the testis. Testes were lysed, 20µg of total protein was loaded per lane, and blots were probed with an antibody against ERK (A) or p-ERK (B). βActin was used as a loading control. Band intensities were quantified using Adobe Photoshop (v.CS2) and the intensity ratio of ERK/βActin (C) and p-ERK/βActin (D) is shown. Values for $Irs2^{+/+}$ were set as 1 arbitrary densitometric unit. Results are mean ± SEM of 4 mice per phenotype. Asterisks denote a significant difference compared to $Irs2^{+/+}$; *** P<0.001.

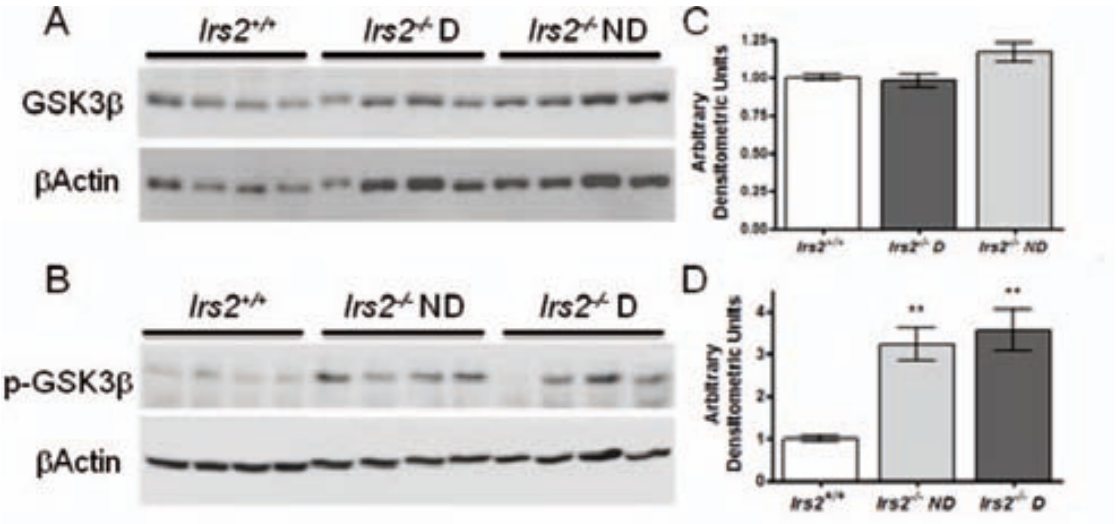

Figure 4.24. Representative immunoblots of GSK3β and p-GSK3β in the testis. Testes were lysed, 20μg of total protein was loaded per lane, and blots were probed with an antibody against GSK3β (A) or p-GSK3β (B). βActin was used as a loading control. Band intensities were quantified using Adobe Photoshop (v.CS2) and the intensity ratio of GSK3β/βActin (C) and p-GSK3β/βActin (D) is shown. Values for $Irs2^{-/-}$ were set as 1 arbitrary densitometric unit. Results are mean ± SEM of 4 mice per phenotype. Asterisks denote a significant difference compared to $Irs2^{+/+}$; ** P<0.01.

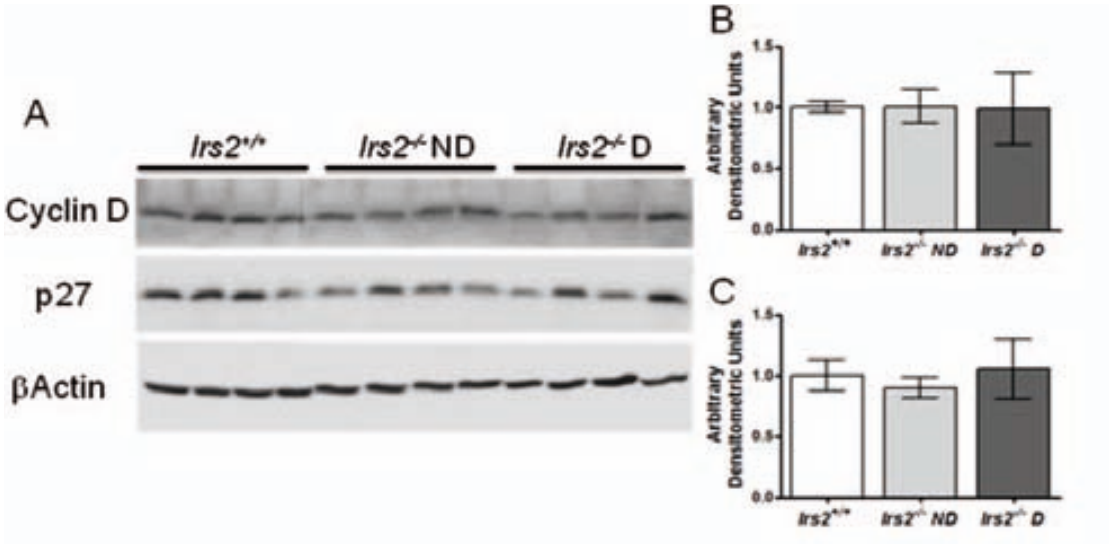

Figure 4.25. Representative immunoblots of cyclin D and p27 in the testis. Testes were lysed, 20μg of total protein was loaded per lane, and blots were probed with an antibody against Cyclin D or p27 (A). βActin was used as a loading control. Band intensities were quantified using Adobe Photoshop (v.CS2) and the intensity ratio of cyclin D/βActin (B) and p27/βActin (C) is shown. Values for $Irs2^{+/+}$ were set as 1 arbitrary densitometric unit. Results are mean ± SEM of 4 mice per phenotype.

Irs2-deficiency does not influence testosterone production

The concentration of testosterone in serum was quantified by ELISA. There were no significant differences between *Irs2*$^{+/+}$, *Irs2*$^{-/-}$ ND, or *Irs2*$^{-/-}$ D mice (Figure 4.26).

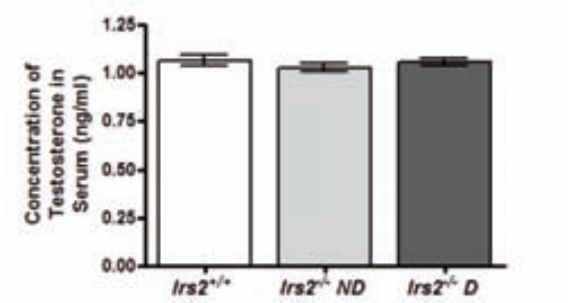

Figure 4.26. Concentrations of testosterone in serum. Testosterone in serum from adult mice was quantified by ELISA. Results are mean ± SEM of 16 *Irs2*$^{+/+}$, 17 *Irs2*$^{-/-}$ ND, and 11 *Irs2*$^{-/-}$ D mice.

Chapter 5 Discussion

In mammals, reproduction is controlled by the hypothalamic-pituitary-gonadal axis but is also influenced by changes in energy homeostasis and metabolism (94). Fertility is closely linked to insulin signaling and glucose metabolism. Previous studies have demonstrated that *Irs2*-deficient mice develop diabetes. Additionally, females are infertile due to reduced pituitary size and gonadotroph numbers, a decrease in concentrations of LH in plasma, and a reduction in ovarian follicles, and consequent anovulation (94). Signaling events downstream of IRS2 in the ovary play critical roles in follicular development and ovulation by regulating key components of the cell cycle apparatus involved in the coordination of proliferation and differentiation (108). The effects of *Irs2* deletion on male reproduction are not well understood. The results of the present project reveal that deletion of *Irs2* causes a significant reduction in the size of the testis; this reduction of size is global since it does not target particular structures or cell populations in the testis but rather diminishes the components proportionally.

The role of IRS2 in testis function was examined initially by comparing testis morphology between $Irs2^{+/+}$ and $Irs2^{-/-}$ mice (Figure 4.1). Visual inspection of male gonads suggested that mice deficient in *Irs2* had smaller testes and this was confirmed by weighing these organs (Table 4.1). Testis weight was reduced by 45% in adult *Irs2*-deficient mice. Consistent with published studies, body weight of $Irs2^{-/-}$ mice was similar to $Irs2^{+/+}$ mice indicating that IRS2 does not affect corporal growth and whole animal development (Table 4.1). However, when testes weight was normalized to body weight, there were significant differences between $Irs2^{+/+}$ and $Irs2^{-/-}$ mice, thereby confirming that *Irs2*-deficiency causes reduced testis size. These observations suggest a previously unknown role for IRS2 in testis development and reproductive function.

Various lines of evidence suggest that both type 1 and type 2 diabetes can lead to impaired male fertility in humans. Hyperglycemia has been shown to reduce the quality of sperm in male diabetic patients (111). There are also other complications of diabetes that can severely impede the ability to reproduce including obesity, fatigue, loss of libido and the inability to maintain an erection (91). The loss of *Irs2* causes diabetes in mice due to pancreatic β cell insufficiency; most male *Irs2*-deficient mice die from diabetic complications by 16 weeks of age (112). However, previous studies have demonstrated that *Irs2*-deficient males are adequate breeders before the onset of severe diabetes (94). Therefore, to establish whether hyperglycemia compounds the effects of *Irs2*-deficiency on male reproduction, transgenic mice were categorized into two groups based on blood glucose levels at the time of sacrifice: $Irs2^{-/-}$ ND (non-diabetic) and $Irs2^{-/-}$ D (diabetic, Table 4.1). Age-matched $Irs2^{+/+}$ mice were used as controls and had normal glucose levels. No differences were observed in testes weight between $Irs2^{-/-}$ ND and $Irs2^{-/-}$ D mice, suggesting that hyperglycemia does not compound the effects of *Irs2* deletion on testis size (Table 4.1). Furthermore, subsequent analysis of testicular cell populations and expression of testicular markers revealed no differences between euglycemic and diabetic *Irs2* null mice. The reduced testis size phenotype is not observed in $Irs2^{+/-}$ males (94), and therefore testes from $Irs2^{+/-}$ mice were not evaluated in these studies.

To characterize the histology of *Irs2*-deficient mice, morphological measurements were taken of the testis, specifically, the diameter and the circumference of seminiferous tubules, and the length of the seminiferous epithelium. Each of these parameters was significantly reduced in *Irs2*-deficient mice compared to $Irs2^{+/+}$ mice (Figure 4.2). Microscopic inspection of testicular cross sections stained with hematoxylin and eosin

revealed that, although each parameter was reduced in size, the organization and structural architecture of the seminiferous epithelium was intact with normal cellular associations, no obvious abnormalities, and elongated spermatids extending into the lumen (Figure 4.1). Testes weights at postnatal day 0 and 4 were significantly reduced in *Irs2*$^{-/-}$ mice, suggesting that the reduced testis size phenotype is a developmental defect (Figures 4.3 and 4.5). Interestingly, this global reduction of organ size without obvious effects on structural organization has also been reported in the brain and kidney: *Irs2*-deficient mice are born with a 35% reduction of brain size (120) and kidney size is reduced by 20% at postnatal day 5 (121). However, although the brain and kidney are noticeably smaller in *Irs2*-deficient mice, all areas are present but reduced proportionally. Collectively, similar observations regarding the developmental effects in testis, brain, and kidney suggest that IRS2 signals are indispensable for specific pathways during critical points of development in these organs.

Sertoli cells play a central role in testicular development as their number determines the size of the testes and the number of germ cells that can be supported during spermatogenesis (51, 52). The expression of the *Sry* gene in the pre-Sertoli cell lineage between E10.5-12.0 initiates Sertoli cell differentiation, committing the gonad to develop as a testis rather than an ovary (122). This activates all downstream pathways which promote the development of a fertile male. One of the first such events is the up-regulation and nuclear localization of transcription factor SOX9 in the male gonad (123). In *Irs2*$^{-/-}$ mice, there were significantly fewer Sertoli cells and accordingly fewer spermatogonia and spermatocytes within cross sections of seminiferous tubules (Figure 4.7A-C). However, when cell numbers were normalized to the diameter of the seminiferous tubules there were no differences between genotypes (Figure 4.8A-C).

The diameter of seminiferous tubules was not different at postnatal day 0, 2, or 4 (Figures 4.3-4.5). During neonatal testicular development, testes weights increase as Sertoli cells proliferate (124). In mice, Sertoli cells cease proliferation by postnatal day 15 (125). Subsequent increases in the diameter and length of seminiferous tubules are due to germ cell proliferation (124). Interestingly, although there were no differences in the expression of the Sertoli cell marker *Gata1,* SOX9 expression was reduced significantly in testes of adult *Irs2*-deficient mice (Figure 4.12B-C). SOX9 is inhibited by Wnt/beta-catenin signaling and various studies indicate that SOX9 expression during testicular development serves to down-regulate Wnt4 (76, 126). In cancer cells, over-expression of IRS1 enhances the expression of SOX9 (127), suggesting that insulin/IGF1 signaling via IRS proteins may oppose Wnt/beta-catenin signals by up-regulating SOX9. The results of the present project are the first to demonstrate a potential connection between IRS2 signals and expression of SOX9 in adult gonads. Thus, one potential explanation for the reduced testis size in this model is that loss of IRS2 signaling modulates SOX9 levels during testis development and/or maturation. The confirmation of this hypothesis will require further studies in cell culture models of Sertoli cells.

In contrast to Sertoli cells, there were significantly more Leydig cells in *Irs2*-deficient mice after data normalization because there were more interstitial spaces per equivalent area (Figure 4.8D). However, this did not correlate with an increased expression of Leydig cell marker *Hsd3b1* (Figure 4.11E). Disruption of the basement membrane leads to defective growth factor and endocrine signaling due to damage to the blood-testis-barrier (128). Staining patterns of smooth muscle actin for peritubular myoid cells and collagen IV, a basement membrane structural component, were not different

between *Irs2*$^{+/+}$ and *Irs2*$^{-/-}$ mice, suggesting that the basement membrane was intact and the blood-testis-barrier was not compromised. In accordance with the normal cellular associations in the seminiferous tubules, these data indicate that spermatogenesis was not compromised in the absence of *Irs2*. Further support for unaltered spermatogenesis and steroidogenesis was found in gene expression studies, since the expression of spermatogonial stem cell marker *Kit*, spermatocyte cell marker *Ddx4,* and *Androgen receptor* were equivalent between mutant and control mice (Figure 4.11).

In humans, conventional semen parameters such as total sperm output, motility, and morphology are not different between diabetic and non-diabetic men. However, there are significantly more nuclear DNA fragmentation and mitochondrial DNA deletions in sperm of diabetic patients (111), suggesting that hyperglycemia and/or altered insulin sensitivity may contribute to deleterious genetic events in sperm of diabetic patients, thereby impairing their reproductive capability. Although the reduced sperm count of *Irs2*-deficient mice reflects a potential reproductive disadvantage, i*n vitro* capacitation of spermatozoa collected from the epididymis revealed that the motility and movement patterns were similar to control mice. These observations suggest that in the absence of IRS2 spermatogenesis proceeds normally and produces morphologically normal spermatozoa, although the absolute numbers are reduced proportionate to reduced testis size. Gene expression studies in the testis indicated that *Irs1, 3,* and *4* were not changed in the absence of *Irs2* (Figure 4.16), suggesting that the other IRS proteins do not compensate for the loss of *Irs2* during testicular development.

Changes in the regulation of cell signaling pathways elicit changes in protein synthesis and cell-cycle control. Surprisingly, expression of PCNA was enhanced in testes of

Irs2$^{-/-}$ mice, despite the reduced size of these organs. This observation may reflect an effort to compensate for retardation of developmental pathways and/or the dysregulation of insulin/IGF1 signaling in the absence of IRS2. In testes of *Irs2*$^{-/-}$ mice, there was an increase in basal p-ERK (Figure 4.23) and p-AKT (Figure 4.22). Another molecule associated with control of growth and proliferation is GSK3β, which is constitutively active and phosphorylates/inactivates multiple target proteins such as cyclin D. Cyclin/CDK complexes function as master integrators that couple mitogenic signaling cascades to the cell cycle and regulate transcription of genes important for G1/S transition and cell cycle progression through the restriction point (87). Insulin signaling leads to the phosphorylation/inactivation of GSK3β by AKT (129). As expected due to the increased phosphorylation of AKT, phosphorylation of GSK3β was enhanced in testes of *Irs2*$^{-/-}$ mice (Figure 4.24). However, there were no differences in cyclin D expression (Figure 4.25). Furthermore, there were no differences in expression of p27, a CDK inhibitor that regulates the G1/S phase transition of the cell cycle (Figure 4.25). The increased basal phosphorylation of AKT and ERK have been reported previously in other tissues of the *Irs2* model and may represent an important component of insulin resistance (130).

A major regulator of tissue growth is GH. Mice lacking GHR secrete normal amounts of GH but are unable to secrete IGF1, which leads to decreased testes weight (131, 132), demonstrating that physiological levels of GH, GHR, and IGF1 are required for normal testis growth (133). Interestingly, gene expression of *Ghr*, which is an indicator of GH action, was significantly decreased in testes of *Irs2* null mice (Figure 4.20E). GH is the key regulator of IGF1 biosynthesis and release and an important modulator of IGF1 actions. In *Irs2*-deficient mice there were significant increases in expression of IGF1R

but not IR (Figure 4.21). Since IGF1 modulates the actions of GH, it is plausible that local production of IGF1R in testes is up-regulated in an attempt to compensate for the reduction in testis size. Sertoli cells express both GHR and IGF1R and produce IGF1 (73) and hence are likely involved in a local mechanism for regulation of testis size.

The insulin signaling pathway is essential for normal growth and development in mice and is composed of three receptors; IR, IGF1R, and IRR. Both IR and IGF1R are necessary for pre- and postnatal growth and development. *Ir* mutant pups die from ketoacidosis within 4 days of birth (134). *Igf1r* mutant mice die at birth due to respiratory failure and exhibit several abnormalities such as reduced size (70). Mice lacking *Ir* and *Igf1r* are even more severely affected (135). In contrast, *Irr* mutant mice are viable and show no observable abnormalities (136). In the absence of the insulin family of receptors, male sex determination during embryonic development is inhibited; the reproductive tracts of *Ir, Igf1r, Irr* triple mutant XY embryos resemble those of XX embryos and exhibit molecular profiles characteristic of females, indicating that testis determination requires insulin signaling (79). One explanation for these effects of impaired IGF1/insulin receptor signaling is the reduction of SRY and SOX9 transcription factors which regulate male sex determination. The fact that loss of *Irs2* also causes a reduction of SOX9 expression suggests that this family of receptors may use IRS2 exclusively for regulation of SOX9.

In summary, the results from these studies demonstrate that IRS2 plays an essential role in the regulation of testis size. Although IRS1 has a critical role in general somatic growth (130), the present data implicate a specific role for IRS2 in the development of certain organs including the testis. The findings of this study suggest that IRS2 may

modulate testis size by reducing or delaying Sertoli cell proliferation during embryonic and early postnatal development. These results provide an important platform for further understanding the effects of IRS2 signaling and diabetes on male reproductive function.

Chapter 6 Conclusions

1. *Irs2*-deficiency causes a reduction of testis size. The weight of the adult testis is reduced by 45% in *Irs2* mutants as compared to control mice. The effects of *Irs2* loss are global, since the structures and cell populations that comprise the testes are reduced proportionally.
2. Reduced testis size associated with *Irs2*-deficiency is apparently an embryonic defect since it was observed during early postnatal development. Consistent with this, the expression of the transcription factor SOX9 was significantly reduced in testes of *Irs2*$^{-/-}$ mice. SOX9 is essential for normal development of the male reproductive system.
3. Spermatogenesis appears to function normally in *Irs2*$^{-/-}$ mice but due to the reduction in testis size, there are fewer cells associated with spermatogenesis and therefore, fewer spermatozoa are produced by *Irs2*$^{-/-}$ males.
4. Capacitated spermatozoa collected from the epididymis of *Irs2*$^{-/-}$ mice exhibit normal motility *in vitro*.
5. No significant differences were observed in testes collected from non-diabetic versus diabetic *Irs2*$^{-/-}$ mice, demonstrating that diabetes and hyperglycemia do not compound the effects of *Irs2* deletion on testis weight or function.
6. The expression of the other members of the IRS protein family (IRS1, 3, and 4) are expressed at normal levels in testes of *Irs2*$^{-/-}$ mice and do not appear to functionally compensate for loss of *Irs2*, providing further support for the specific and essential role of IRS2 in testis development.
7. The expression of IGF1R, but not IR, was up-regulated in *Irs2*$^{-/-}$ mice. Consistent with this, basal phosphorylation of the downstream elements AKT and MAPK were enhanced in adult *Irs2*-deficient testes. The expression of the

proliferation marker PCNA was also increased. Collectively, these results suggest that IGF1R-mediated signaling may attempt to compensate for the absence of *Irs2*.

8. Steroidogenesis is apparently normal in *Irs2*-deficient testes since circulating levels of testosterone and gene expression levels of androgen receptor and 3β-hydroxysteroid dehydrogenase were comparable to control mice. The significance of increased expression of the LH and FSH receptor in $Irs2^{-/-}$ mice will require further study.

References

1. **Pessin JE, Saltiel AR** 2000 Signaling pathways in insulin action: molecular targets of insulin resistance. J Clin Invest 106:165-169
2. **Kanzaki M, Pessin JE** 2001 Signal integration and the specificity of insulin action. Cell Biochem Biophys 35:191-209
3. **Kahn CR, White MF** 1988 The insulin receptor and the molecular mechanism of insulin action. J Clin Invest 82:1151-1156
4. **Rinderknecht E, Humbel RE** 1978 The amino acid sequence of human insulin-like growth factor I and its structural homology with proinsulin. J Biol Chem 253:2769-2776
5. **Hwa V, Oh Y, Rosenfeld RG** 1999 The insulin-like growth factor-binding protein (IGFBP) superfamily. Endocr Rev 20:761-787
6. **Laron Z** 2001 Insulin-like growth factor 1 (IGF-1): a growth hormone. Mol Pathol 54:311-316
7. **Laron Z** 1999 Somatomedin-1 (recombinant insulin-like growth factor-1): clinical pharmacology and potential treatment of endocrine and metabolic disorders. BioDrugs 11:55-70
8. **Favelyukis S, Till JH, Hubbard SR, Miller WT** 2001 Structure and autoregulation of the insulin-like growth factor 1 receptor kinase. Nat Struct Biol 8:1058-1063
9. **White MF** 1997 The insulin signalling system and the IRS proteins. Diabetologia 40 Suppl 2:S2-17
10. **Ullrich A, Schlessinger J** 1990 Signal transduction by receptors with tyrosine kinase activity. Cell 61:203-212
11. **Friedman JE, Ishizuka T, Liu S, Farrell CJ, Bedol D, Koletsky RJ, Kaung HL, Ernsberger P** 1997 Reduced insulin receptor signaling in the obese spontaneously hypertensive Koletsky rat. Am J Physiol 273:E1014-1023
12. **Klammt J, Garten A, Barnikol-Oettler A, Beck-Sickinger AG, Kiess W** 2005 Comparative analysis of the signaling capabilities of the insulin receptor-related receptor. Biochem Biophys Res Commun 327:557-564
13. **Hanke S, Mann M** 2009 The phosphotyrosine interactome of the insulin receptor family and its substrates IRS-1 and IRS-2. Mol Cell Proteomics 8:519-534
14. **Withers DJ** 2001 Insulin receptor substrate proteins and neuroendocrine function. Biochem Soc Trans 29:525-529
15. **Taniguchi CM, Emanuelli B, Kahn CR** 2006 Critical nodes in signalling pathways: insights into insulin action. Nat Rev Mol Cell Biol 7:85-96
16. **Wu J, Tseng YD, Xu CF, Neubert TA, White MF, Hubbard SR** 2008 Structural and biochemical characterization of the KRLB region in insulin receptor substrate-2. Nat Struct Mol Biol 15:251-258
17. **Biddinger SB, Kahn CR** 2006 From mice to men: insights into the insulin resistance syndromes. Annu Rev Physiol 68:123-158
18. **Voliovitch H, Schindler DG, Hadari YR, Taylor SI, Accili D, Zick Y** 1995 Tyrosine phosphorylation of insulin receptor substrate-1 in vivo depends upon the presence of its pleckstrin homology region. J Biol Chem 270:18083-18087
19. **Boura-Halfon S, Zick Y** 2009 Phosphorylation of IRS proteins, insulin action, and insulin resistance. Am J Physiol Endocrinol Metab 296:E581-591
20. **Kahn CR, White MF, Shoelson SE, Backer JM, Araki E, Cheatham B, Csermely P, Folli F, Goldstein BJ, Huertas P, et al.** 1993 The insulin receptor

and its substrate: molecular determinants of early events in insulin action. Recent Prog Horm Res 48:291-339

21. **Skolnik EY, Lee CH, Batzer A, Vicentini LM, Zhou M, Daly R, Myers MJ, Jr., Backer JM, Ullrich A, White MF, et al.** 1993 The SH2/SH3 domain-containing protein GRB2 interacts with tyrosine-phosphorylated IRS1 and Shc: implications for insulin control of ras signalling. Embo J 12:1929-1936
22. **Backer JM, Myers MG, Jr., Shoelson SE, Chin DJ, Sun XJ, Miralpeix M, Hu P, Margolis B, Skolnik EY, Schlessinger J, et al.** 1992 Phosphatidylinositol 3'-kinase is activated by association with IRS-1 during insulin stimulation. Embo J 11:3469-3479
23. **Giorgetti S, Pelicci PG, Pelicci G, Van Obberghen E** 1994 Involvement of Src-homology/collagen (SHC) proteins in signaling through the insulin receptor and the insulin-like-growth-factor-I-receptor. Eur J Biochem 223:195-202
24. **Holgado-Madruga M, Emlet DR, Moscatello DK, Godwin AK, Wong AJ** 1996 A Grb2-associated docking protein in EGF- and insulin-receptor signalling. Nature 379:560-564
25. **Myers MG, Jr., Backer JM, Sun XJ, Shoelson S, Hu P, Schlessinger J, Yoakim M, Schaffhausen B, White MF** 1992 IRS-1 activates phosphatidylinositol 3'-kinase by associating with src homology 2 domains of p85. Proc Natl Acad Sci U S A 89:10350-10354
26. **James SR, Downes CP, Gigg R, Grove SJ, Holmes AB, Alessi DR** 1996 Specific binding of the Akt-1 protein kinase to phosphatidylinositol 3,4,5-trisphosphate without subsequent activation. Biochem J 315 (Pt 3):709-713
27. **Komander D, Fairservice A, Deak M, Kular GS, Prescott AR, Peter Downes C, Safrany ST, Alessi DR, van Aalten DM** 2004 Structural insights into the regulation of PDK1 by phosphoinositides and inositol phosphates. Embo J 23:3918-3928
28. **Alessi DR, James SR, Downes CP, Holmes AB, Gaffney PR, Reese CB, Cohen P** 1997 Characterization of a 3-phosphoinositide-dependent protein kinase which phosphorylates and activates protein kinase Balpha. Curr Biol 7:261-269
29. **Cantley LC** 2002 The phosphoinositide 3-kinase pathway. Science 296:1655-1657
30. **Armstrong CG, Doherty MJ, Cohen PT** 1998 Identification of the separate domains in the hepatic glycogen-targeting subunit of protein phosphatase 1 that interact with phosphorylase a, glycogen and protein phosphatase 1. Biochem J 336 (Pt 3):699-704
31. **Kitamura T, Kitamura Y, Kuroda S, Hino Y, Ando M, Kotani K, Konishi H, Matsuzaki H, Kikkawa U, Ogawa W, Kasuga M** 1999 Insulin-induced phosphorylation and activation of cyclic nucleotide phosphodiesterase 3B by the serine-threonine kinase Akt. Mol Cell Biol 19:6286-6296
32. **Lefebvre V, Mechin MC, Louckx MP, Rider MH, Hue L** 1996 Signaling pathway involved in the activation of heart 6-phosphofructo-2-kinase by insulin. J Biol Chem 271:22289-22292
33. **Kimura KD, Tissenbaum HA, Liu Y, Ruvkun G** 1997 daf-2, an insulin receptor-like gene that regulates longevity and diapause in Caenorhabditis elegans. Science 277:942-946
34. **Cohen P** 2006 The twentieth century struggle to decipher insulin signalling. Nat Rev Mol Cell Biol 7:867-873

35. **Plotnikov A, Zehorai E, Procaccia S, Seger R** 2011 The MAPK cascades: signaling components, nuclear roles and mechanisms of nuclear translocation. Biochim Biophys Acta 1813:1619-1633
36. **Yoon S, Seger R** 2006 The extracellular signal-regulated kinase: multiple substrates regulate diverse cellular functions. Growth Factors 24:21-44
37. **Tanti JF, Jager J** 2009 Cellular mechanisms of insulin resistance: role of stress-regulated serine kinases and insulin receptor substrates (IRS) serine phosphorylation. Curr Opin Pharmacol 9:753-762
38. **Mori H, Christensen AK** 1980 Morphometric analysis of Leydig cells in the normal rat testis. J Cell Biol 84:340-354
39. **Russell LD ER, Sinha Hikim AP, Clegg ED** 1990 Histological and Histopathological Evaluation of the Testis. Clearwater, FL, USA: Cache River Press
40. **Russell LD, Saxena NK, Turner TT** 1989 Cytoskeletal involvement in spermiation and sperm transport. Tissue Cell 21:361-379
41. **Holstein AF, Maekawa M, Nagano T, Davidoff MS** 1996 Myofibroblasts in the lamina propria of human semi-niferous tubules are dynamic structures of heterogeneous phenotype. Arch Histol Cytol 59:109-125
42. **Wagner MS, Wajner SM, Maia AL** 2008 The role of thyroid hormone in testicular development and function. J Endocrinol 199:351-365
43. **Yan HH, Mruk DD, Cheng CY** 2008 Junction restructuring and spermatogenesis: the biology, regulation, and implication in male contraceptive development. Curr Top Dev Biol 80:57-92
44. **Holstein AF, Schulze W, Davidoff M** 2003 Understanding spermatogenesis is a prerequisite for treatment. Reprod Biol Endocrinol 1:107
45. **Phillips BT, Gassei K, Orwig KE** 2010 Spermatogonial stem cell regulation and spermatogenesis. Philos Trans R Soc Lond B Biol Sci 365:1663-1678
46. **Clermont Y** 1972 Kinetics of spermatogenesis in mammals: seminiferous epithelium cycle and spermatogonial renewal. Physiol Rev 52:198-236
47. **Hecht NB** 1998 Molecular mechanisms of male germ cell differentiation. Bioessays 20:555-561
48. **Eddy EM, O'Brien DA** 1998 Gene expression during mammalian meiosis. Curr Top Dev Biol 37:141-200
49. **Plante G, Therien I, Manjunath P** 2012 Characterization of Recombinant Murine Binder of Sperm Protein Homolog 1 and Its Role in Capacitation. Biol Reprod
50. **Mackay S** 2000 Gonadal development in mammals at the cellular and molecular levels. Int Rev Cytol 200:47-99
51. **Sharpe RM, McKinnell C, Kivlin C, Fisher JS** 2003 Proliferation and functional maturation of Sertoli cells, and their relevance to disorders of testis function in adulthood. Reproduction 125:769-784
52. **Orth JM, Gunsalus GL, Lamperti AA** 1988 Evidence from Sertoli cell-depleted rats indicates that spermatid number in adults depends on numbers of Sertoli cells produced during perinatal development. Endocrinology 122:787-794
53. **Wang ZX, Wreford NG, De Kretser DM** 1989 Determination of Sertoli cell numbers in the developing rat testis by stereological methods. Int J Androl 12:58-64
54. **Griswold MD** 1998 The central role of Sertoli cells in spermatogenesis. Semin Cell Dev Biol 9:411-416

55. **Holsberger DR, Kiesewetter SE, Cooke PS** 2005 Regulation of neonatal Sertoli cell development by thyroid hormone receptor alpha1. Biol Reprod 73:396-403
56. **Quigley CA, De Bellis A, Marschke KB, el-Awady MK, Wilson EM, French FS** 1995 Androgen receptor defects: historical, clinical, and molecular perspectives. Endocr Rev 16:271-321
57. **Payne AH HM, Russell LD** 1996 The Leydig Cell. Vienna, IL, USA: Cache River Press
58. **McLachlan RI, O'Donnell L, Meachem SJ, Stanton PG, de Kretser DM, Pratis K, Robertson DM** 2002 Identification of specific sites of hormonal regulation in spermatogenesis in rats, monkeys, and man. Recent Prog Horm Res 57:149-179
59. **Huhtaniemi I, Toppari J** 1995 Endocrine, paracrine and autocrine regulation of testicular steroidogenesis. Adv Exp Med Biol 377:33-54
60. **Dufau ML** 1988 Endocrine regulation and communicating functions of the Leydig cell. Annu Rev Physiol 50:483-508
61. **Shiraishi K, Ascoli M** 2007 Lutropin/choriogonadotropin stimulate the proliferation of primary cultures of rat Leydig cells through a pathway that involves activation of the extracellularly regulated kinase 1/2 cascade. Endocrinology 148:3214-3225
62. **Spiteri-Grech J, Nieschlag E** 1992 The role of growth hormone and insulin-like growth factor I in the regulation of male reproductive function. Horm Res 38 Suppl 1:22-27
63. **Zachmann M** 1992 Interrelations between growth hormone and sex hormones: physiology and therapeutic consequences. Horm Res 38 Suppl 1:1-8
64. **Franks S** 1998 Growth hormone and ovarian function. Baillieres Clin Endocrinol Metab 12:331-340
65. **Pantaleon M, Whiteside EJ, Harvey MB, Barnard RT, Waters MJ, Kaye PL** 1997 Functional growth hormone (GH) receptors and GH are expressed by preimplantation mouse embryos: a role for GH in early embryogenesis? Proc Natl Acad Sci U S A 94:5125-5130
66. **Fowden AL** 1995 Endocrine regulation of fetal growth. Reprod Fertil Dev 7:351-363
67. **Efstratiadis A** 1998 Genetics of mouse growth. Int J Dev Biol 42:955-976
68. **DeChiara TM, Efstratiadis A, Robertson EJ** 1990 A growth-deficiency phenotype in heterozygous mice carrying an insulin-like growth factor II gene disrupted by targeting. Nature 345:78-80
69. **DeChiara TM, Robertson EJ, Efstratiadis A** 1991 Parental imprinting of the mouse insulin-like growth factor II gene. Cell 64:849-859
70. **Liu JP, Baker J, Perkins AS, Robertson EJ, Efstratiadis A** 1993 Mice carrying null mutations of the genes encoding insulin-like growth factor I (Igf-1) and type 1 IGF receptor (Igf1r). Cell 75:59-72
71. **Baker J, Liu JP, Robertson EJ, Efstratiadis A** 1993 Role of insulin-like growth factors in embryonic and postnatal growth. Cell 75:73-82
72. **Nyberg F, Burman P** 1996 Growth hormone and its receptors in the central nervous system--location and functional significance. Horm Res 45:18-22
73. **Lobie PE, Breipohl W, Aragon JG, Waters MJ** 1990 Cellular localization of the growth hormone receptor/binding protein in the male and female reproductive systems. Endocrinology 126:2214-2221

74. **Schneider HJ, Pagotto U, Stalla GK** 2003 Central effects of the somatotropic system. Eur J Endocrinol 149:377-392
75. **Chandrashekar V, Zaczek D, Bartke A** 2004 The consequences of altered somatotropic system on reproduction. Biol Reprod 71:17-27
76. **Maatouk DM, DiNapoli L, Alvers A, Parker KL, Taketo MM, Capel B** 2008 Stabilization of beta-catenin in XY gonads causes male-to-female sex-reversal. Hum Mol Genet 17:2949-2955
77. **Tevosian SG, Albrecht KH, Crispino JD, Fujiwara Y, Eicher EM, Orkin SH** 2002 Gonadal differentiation, sex determination and normal Sry expression in mice require direct interaction between transcription partners GATA4 and FOG2. Development 129:4627-4634
78. **Albrecht KH, Young M, Washburn LL, Eicher EM** 2003 Sry expression level and protein isoform differences play a role in abnormal testis development in C57BL/6J mice carrying certain Sry alleles. Genetics 164:277-288
79. **Nef S, Verma-Kurvari S, Merenmies J, Vassalli JD, Efstratiadis A, Accili D, Parada LF** 2003 Testis determination requires insulin receptor family function in mice. Nature 426:291-295
80. **Kashimada K, Koopman P** 2010 Sry: the master switch in mammalian sex determination. Development 137:3921-3930
81. **Yomogida K, Ohtani H, Harigae H, Ito E, Nishimune Y, Engel JD, Yamamoto M** 1994 Developmental stage- and spermatogenic cycle-specific expression of transcription factor GATA-1 in mouse Sertoli cells. Development 120:1759-1766
82. **Wu JC, Gregory CW, DePhilip RM** 1993 Expression of E-cadherin in immature rat and mouse testis and in rat Sertoli cell cultures. Biol Reprod 49:1353-1361
83. **Lobo MV, Arenas MI, Alonso FJ, Gomez G, Bazan E, Paino CL, Fernandez E, Fraile B, Paniagua R, Moyano A, Caso E** 2004 Nestin, a neuroectodermal stem cell marker molecule, is expressed in Leydig cells of the human testis and in some specific cell types from human testicular tumours. Cell Tissue Res 316:369-376
84. **Hickford DE, Frankenberg S, Pask AJ, Shaw G, Renfree MB** 2011 DDX4 (VASA) is conserved in germ cell development in marsupials and monotremes. Biol Reprod 85:733-743
85. **Maga G, Hubscher U** 2003 Proliferating cell nuclear antigen (PCNA): a dancer with many partners. J Cell Sci 116:3051-3060
86. **Feng LX, Ravindranath N, Dym M** 2000 Stem cell factor/c-kit up-regulates cyclin D3 and promotes cell cycle progression via the phosphoinositide 3-kinase/p70 S6 kinase pathway in spermatogonia. J Biol Chem 275:25572-25576
87. **Lange CA, Yee D** 2011 Killing the second messenger: targeting loss of cell cycle control in endocrine-resistant breast cancer. Endocr Relat Cancer 18:C19-24
88. **Walters KA, Allan CM, Handelsman DJ** 2012 Rodent Models for Human Polycystic Ovary Syndrome. Biol Reprod
89. **Sharpe RM** 2010 Environmental/lifestyle effects on spermatogenesis. Philos Trans R Soc Lond B Biol Sci 365:1697-1712
90. **Sabatini ME, Guo L, Lynch MP, Doyle JO, Lee H, Rueda BR, Styer AK** 2011 Metformin therapy in a hyperandrogenic anovulatory mutant murine model with polycystic ovarian syndrome characteristics improves oocyte maturity during superovulation. J Ovarian Res 4:8

91. **Mah PM, Wittert GA** 2010 Obesity and testicular function. Mol Cell Endocrinol 316:180-186
92. **Field AE, Coakley EH, Must A, Spadano JL, Laird N, Dietz WH, Rimm E, Colditz GA** 2001 Impact of overweight on the risk of developing common chronic diseases during a 10-year period. Arch Intern Med 161:1581-1586
93. **La Vignera S, Condorelli RA, Vicari E, D'Agata R, Salemi M, Calogero AE** 2011 High levels of lipid peroxidation in semen of diabetic patients. Andrologia
94. **Burks DJ, Font de Mora J, Schubert M, Withers DJ, Myers MG, Towery HH, Altamuro SL, Flint CL, White MF** 2000 IRS-2 pathways integrate female reproduction and energy homeostasis. Nature 407:377-382
95. **Hammoud AO, Gibson M, Peterson CM, Meikle AW, Carrell DT** 2008 Impact of male obesity on infertility: a critical review of the current literature. Fertil Steril 90:897-904
96. **Magnusdottir EV, Thorsteinsson T, Thorsteinsdottir S, Heimisdottir M, Olafsdottir K** 2005 Persistent organochlorines, sedentary occupation, obesity and human male subfertility. Hum Reprod 20:208-215
97. **Jensen TK, Andersson AM, Jorgensen N, Andersen AG, Carlsen E, Petersen JH, Skakkebaek NE** 2004 Body mass index in relation to semen quality and reproductive hormones among 1,558 Danish men. Fertil Steril 82:863-870
98. **Kort HI, Massey JB, Elsner CW, Mitchell-Leef D, Shapiro DB, Witt MA, Roudebush WE** 2006 Impact of body mass index values on sperm quantity and quality. J Androl 27:450-452
99. **Nielsen TL, Hagen C, Wraae K, Brixen K, Petersen PH, Haug E, Larsen R, Andersen M** 2007 Visceral and subcutaneous adipose tissue assessed by magnetic resonance imaging in relation to circulating androgens, sex hormone-binding globulin, and luteinizing hormone in young men. J Clin Endocrinol Metab 92:2696-2705
100. **Raman JD, Schlegel PN** 2002 Aromatase inhibitors for male infertility. J Urol 167:624-629
101. **Winters SJ, Wang C, Abdelrahaman E, Hadeed V, Dyky MA, Brufsky A** 2006 Inhibin-B levels in healthy young adult men and prepubertal boys: is obesity the cause for the contemporary decline in sperm count because of fewer Sertoli cells? J Androl 27:560-564
102. **Shafik A, Olfat S** 1981 Scrotal lipomatosis. Br J Urol 53:50-54
103. **Choudhury AI, Heffron H, Smith MA, Al-Qassab H, Xu AW, Selman C, Simmgen M, Clements M, Claret M, Maccoll G, Bedford DC, Hisadome K, Diakonov I, Moosajee V, Bell JD, Speakman JR, Batterham RL, Barsh GS, Ashford ML, Withers DJ** 2005 The role of insulin receptor substrate 2 in hypothalamic and beta cell function. J Clin Invest 115:940-950
104. **Bruning JC, Gautam D, Burks DJ, Gillette J, Schubert M, Orban PC, Klein R, Krone W, Muller-Wieland D, Kahn CR** 2000 Role of brain insulin receptor in control of body weight and reproduction. Science 289:2122-2125
105. **Burcelin R, Thorens B, Glauser M, Gaillard RC, Pralong FP** 2003 Gonadotropin-releasing hormone secretion from hypothalamic neurons: stimulation by insulin and potentiation by leptin. Endocrinology 144:4484-4491
106. **Kovacs P, Morales JC, Karkanias GB** 2003 Central insulin administration maintains reproductive behavior in diabetic female rats. Neuroendocrinology 78:90-95

107. **Salvi R, Castillo E, Voirol MJ, Glauser M, Rey JP, Gaillard RC, Vollenweider P, Pralong FP** 2006 Gonadotropin-releasing hormone-expressing neurons immortalized conditionally are activated by insulin: implication of the mitogen-activated protein kinase pathway. Endocrinology 147:816-826
108. **Neganova I, Al-Qassab H, Heffron H, Selman C, Choudhury AI, Lingard SJ, Diakonov I, Patterson M, Ghatei M, Bloom SR, Franks S, Huhtaniemi I, Hardy K, Withers DJ** 2007 Role of central nervous system and ovarian insulin receptor substrate 2 signaling in female reproductive function in the mouse. Biol Reprod 76:1045-1053
109. **Franks S, Gilling-Smith C, Watson H, Willis D** 1999 Insulin action in the normal and polycystic ovary. Endocrinol Metab Clin North Am 28:361-378
110. **Thakur M, Chauhan NS, Sharma V, Dixit VK, Bhargava S** 2012 Effect of Curculigo orchioides on hyperglycemia-induced oligospermia and sexual dysfunction in male rats. Int J Impot Res 24:31-37
111. **Agbaje IM, Rogers DA, McVicar CM, McClure N, Atkinson AB, Mallidis C, Lewis SE** 2007 Insulin dependant diabetes mellitus: implications for male reproductive function. Hum Reprod 22:1871-1877
112. **Withers DJ, Gutierrez JS, Towery H, Burks DJ, Ren JM, Previs S, Zhang Y, Bernal D, Pons S, Shulman GI, Bonner-Weir S, White MF** 1998 Disruption of IRS-2 causes type 2 diabetes in mice. Nature 391:900-904
113. **Sesti G, Federici M, Hribal ML, Lauro D, Sbraccia P, Lauro R** 2001 Defects of the insulin receptor substrate (IRS) system in human metabolic disorders. Faseb J 15:2099-2111
114. **Tamemoto H, Kadowaki T, Tobe K, Yagi T, Sakura H, Hayakawa T, Terauchi Y, Ueki K, Kaburagi Y, Satoh S, et al.** 1994 Insulin resistance and growth retardation in mice lacking insulin receptor substrate-1. Nature 372:182-186
115. **Araki E, Lipes MA, Patti ME, Bruning JC, Haag B, 3rd, Johnson RS, Kahn CR** 1994 Alternative pathway of insulin signalling in mice with targeted disruption of the IRS-1 gene. Nature 372:186-190
116. **Liu SC, Wang Q, Lienhard GE, Keller SR** 1999 Insulin receptor substrate 3 is not essential for growth or glucose homeostasis. J Biol Chem 274:18093-18099
117. **Fantin VR, Wang Q, Lienhard GE, Keller SR** 2000 Mice lacking insulin receptor substrate 4 exhibit mild defects in growth, reproduction, and glucose homeostasis. Am J Physiol Endocrinol Metab 278:E127-133
118. **Schmittgen TD, Livak KJ** 2008 Analyzing real-time PCR data by the comparative C(T) method. Nat Protoc 3:1101-1108
119. **Welsh M, Saunders PT, Atanassova N, Sharpe RM, Smith LB** 2009 Androgen action via testicular peritubular myoid cells is essential for male fertility. Faseb J 23:4218-4230
120. **Schubert M, Brazil DP, Burks DJ, Kushner JA, Ye J, Flint CL, Farhang-Fallah J, Dikkes P, Warot XM, Rio C, Corfas G, White MF** 2003 Insulin receptor substrate-2 deficiency impairs brain growth and promotes tau phosphorylation. J Neurosci 23:7084-7092
121. **Carew RM, Sadagurski M, Goldschmeding R, Martin F, White MF, Brazil DP** 2010 Deletion of Irs2 causes reduced kidney size in mice: role for inhibition of GSK3beta? BMC Dev Biol 10:73
122. **Sekido R, Lovell-Badge R** 2009 Sex determination and SRY: down to a wink and a nudge? Trends Genet 25:19-29

123. **Sekido R, Bar I, Narvaez V, Penny G, Lovell-Badge R** 2004 SOX9 is up-regulated by the transient expression of SRY specifically in Sertoli cell precursors. Dev Biol 274:271-279
124. **Franca LR, Silva VA, Jr., Chiarini-Garcia H, Garcia SK, Debeljuk L** 2000 Cell proliferation and hormonal changes during postnatal development of the testis in the pig. Biol Reprod 63:1629-1636
125. **Vergouwen RP, Jacobs SG, Huiskamp R, Davids JA, de Rooij DG** 1991 Proliferative activity of gonocytes, Sertoli cells and interstitial cells during testicular development in mice. J Reprod Fertil 93:233-243
126. **Tamashiro DA, Alarcon VB, Marikawa Y** 2008 Ectopic expression of mouse Sry interferes with Wnt/beta-catenin signaling in mouse embryonal carcinoma cell lines. Biochim Biophys Acta 1780:1395-1402
127. **Ramocki NM, Wilkins HR, Magness ST, Simmons JG, Scull BP, Lee GH, McNaughton KK, Lund PK** 2008 Insulin receptor substrate-1 deficiency promotes apoptosis in the putative intestinal crypt stem cell region, limits Apcmin/+ tumors, and regulates Sox9. Endocrinology 149:261-267
128. **Gruber M, Mathew LK, Runge AC, Garcia JA, Simon MC** 2010 EPAS1 Is Required for Spermatogenesis in the Postnatal Mouse Testis. Biol Reprod 82:1227-1236
129. **Fingar DC, Salama S, Tsou C, Harlow E, Blenis J** 2002 Mammalian cell size is controlled by mTOR and its downstream targets S6K1 and 4EBP1/eIF4E. Genes Dev 16:1472-1487
130. **Withers DJ, Burks DJ, Towery HH, Altamuro SL, Flint CL, White MF** 1999 Irs-2 coordinates Igf-1 receptor-mediated beta-cell development and peripheral insulin signalling. Nat Genet 23:32-40
131. **Chandrashekar V, Bartke A, Coschigano KT, Kopchick JJ** 1999 Pituitary and testicular function in growth hormone receptor gene knockout mice. Endocrinology 140:1082-1088
132. **Zhou Y, Xu BC, Maheshwari HG, He L, Reed M, Lozykowski M, Okada S, Cataldo L, Coschigamo K, Wagner TE, Baumann G, Kopchick JJ** 1997 A mammalian model for Laron syndrome produced by targeted disruption of the mouse growth hormone receptor/binding protein gene (the Laron mouse). Proc Natl Acad Sci U S A 94:13215-13220
133. **Chandrashekar V, Bartke A, Awoniyi CA, Tsai-Morris CH, Dufau ML, Russell LD, Kopchick JJ** 2001 Testicular endocrine function in GH receptor gene disrupted mice. Endocrinology 142:3443-3450
134. **Accili D, Drago J, Lee EJ, Johnson MD, Cool MH, Salvatore P, Asico LD, Jose PA, Taylor SI, Westphal H** 1996 Early neonatal death in mice homozygous for a null allele of the insulin receptor gene. Nat Genet 12:106-109
135. **Louvi A, Accili D, Efstratiadis A** 1997 Growth-promoting interaction of IGF-II with the insulin receptor during mouse embryonic development. Dev Biol 189:33-48
136. **Kitamura T, Kido Y, Nef S, Merenmies J, Parada LF, Accili D** 2001 Preserved pancreatic beta-cell development and function in mice lacking the insulin receptor-related receptor. Mol Cell Biol 21:5624-5630